A Framework for Ship Stability in a Seastate using the State-Space Fokker-Planck Method

by

David F. H. Larson

B.S. Mechanical Engineering
Massachusetts Institute of Technology, 2016

Submitted to the Department of Mechanical Engineering
in partial fulfillment of the requirements for the degree of

Master of Science in Mechanical Engineering

at the

MASSACHUSETTS INSTITUTE OF TECHNOLOGY

June 2018

Author ..... Signature redacted .....
Department of Mechanical Engineering
May 11, 2018

Certified by ..... Signature redacted
Paul D. Sclavounos
Professor of Mechanical Engineering & Naval Architecture
Thesis Supervisor

Accepted by ..... Signature redacted
Rohan Abeyaratne
Chair, Department Committee on Graduate Students

A Framework for Ship Stability in a Seastate using the State-Space Fokker-Planck Method

by

David F. H. Larson

Submitted to the Department of Mechanical Engineering,
on May 11, 2018, in partial fulfillment of the
requirements for the degree of
Master of Science in Mechanical Engineering

Abstract

Ships sailing on the ocean have many inherent dangers. One of the most compelling is when they interact with severe stochastic waves, resulting in a loss of stability and adversely affecting their operation. This can result in extreme motions, at the very least making life difficult for crew, to potentially the most catastrophic events—capsize, and loss of cargo and life. This compels the need to reliably predict vessel responses to wave interactions in order to aid the decision-making process for operating the ship safely. Despite the advances in computational methods and stochastic-hydrodynamic theories to this date, a general framework, capable of handling nonlinear three-dimensional effects, arbitrary wave headings and unconventional hull geometries, is still missing from the engineer's toolbox.

This thesis presents a new methodology for modeling the nonlinear responses and stability of a ship in stochastic waves. Invoking the weak-scatterer hypothesis, the radiation and diffraction effects are linearized, computed via a panel method, and cast into a state-space form, aided by applying the ESPRIT algorithm. Strong free-surface nonlinearities present in the Froude-Krylov exciting and hydrostatic restoring forces are modeled by Fluid Impulse Theory. In parallel, the ambient seastate is represented by a multidimensional stochastic differential equation (SDE) conforming to a prescribed spectrum. Combining the state-space and seastate models capacitates the study of the nonlinear seakeeping and stability of a ship in a broad range of stationary seastates via stochastic calculus methods. Chief among them is the use of the Fokker-Planck equation (FPE), a deterministic partial differential equation governing the joint probability density function of the states of the SDE. The formulation

for a rectangular barge rolling in beam waves is presented, with the approach readily extendable to six-degree-of-freedom responses. By deriving a state-space stochastic differential equation for the states governing the vessel response motions, the joint probability density can be found either by numerical Monte-Carlo simulation of the SDE, or by numerically solving the associated FPE.

Thesis Supervisor: Paul D. Sclavounos
Title: Professor of Mechanical Engineering & Naval Architecture

Acknowledgments

I express my sincere gratitude to Professor Paul Sclavounos for the mentorship and guidance he has provided me since joining his lab as a UROP. His encouragement, inside the "box" and out, has been a critical component in my growth as an engineer, scientist, naval architect and person.

I owe a great deal of thanks to all of my friends and mentors for their advice, encouragement and support. To Paige, David, João, Sameena, Moseley, Colin, Patrick, Trevor, Amanda, Jaqueline, Duncan, Doug and Fran, just to name a few, for contributing to my growth and creativity in all walks of life, and keeping me sane day in, and day out. To my lab mates, Emily and Yu, for all of the discussions and advice on any problem we encountered. And to my parents and sister for their unconditional love and steady supply of cookies. It has been a genuinely fantastic time.

This research was financially supported by the Office of Naval Research under Grant N00014-16-1-3031.

Contents

List of Figures

List of Tables

Chapter 1

Introduction

Vessels operating on the open ocean are an integral part of human society—of transit, commerce, exploration and defense. The vessels and activities range from pleasure craft at small scale, commercial fishing and offshore enterprise at medium scale, to cargo shipping and naval vessel activities at the largest scale, and withal, first-response rescue in the event of disaster. Particularly the latter three must face the awesome and often unpredictable nature of the ocean—operating in an environment where extreme seastates and storms are commonplace. Consequences of operating in severe seastates range from crew discomfort and reduced mission efficacy to catastrophic structural failures and capsize that may lead to the loss of the vessel [1]. The alternative is to attempt to use advanced weather forecasting and geospatial navigation to plot courses around storm regions, or to even not venture out. However, the costs of sailing a weather-evasive course can be astronomical in terms of lost time for cargo loads or naval mission success[1, 2]. Increased fuel burn, added crew hours, consumption of resources and stratospheric insurance costs, to name a few factors, compound quickly. Even accepting these costs, there's always a possibility

of encountering severe weather, due to the uncertainty and complexity of the ocean environment [1, 3, 4].

As we design unconventional hull geometries and novel mission requirements for severe weather, the ship behavior becomes evermore complex. We desire to better understand the boundaries of stable operation so that we may approach our mission safely and confidently without needlessly impacting our bottom line. To do so, we are driven to better understand the theory of how ships respond to stochastic ocean waves in a more general and all-encompassing form than we currently have. This work aims to introduce a novel unified approach to analyzing the statistical nature of ship responses, including nonlinear effects, subject to severe stochastic seastates, without any specification or restriction on the types of geometries allowed. Thereby, we may better understand the new designs we wish to put out on the ocean.

1.1 The Ship Stability Problem

Vessels operating in random waves may experience large responses and loss of stability. However, it is challenging to predict exactly when this may happen. The past several decades have seen appreciable progress towards developing potential and viscous hydrodynamic computational methods for analyzing the linear and nonlinear seakeeping behavior of these ships. Combining these methods with experiments and real-world data has been the primary tool for treating the ship stability problem in realistic environments [1]. Additionally, a handful of useful theoretical models have been proposed and implemented for estimating the likelihood of extreme motion and capsize, such as split-time methods [5], envelope-peaks-over-threshold and confidence interval approaches [6], and others based on (non)linear oscillators. While powerful for the primary destabilizing modes, these methods are dominantly constrained to a

single-degree-of-freedom, planar motion, or special cases, such as rolling in beam-seas and parametric rolling. Furthermore, some call for challenging modeling decisions to be made on a case-by-case basis, and others require parameters that may be challenging to estimate in early design phases.

As such, we still lack a general purpose theoretical framework to asses the stability properties of ships. These studies require explicit accounting of nonlinearities of both potential and viscous origin, complete coupling of the modes of motion, and developing statistical models for the nonlinear ship responses and their extreme statistics in a stochastic seastate. Such studies are typically carried out by Monte-Carlo simulations to determine the Safe Operating Envelope. This approach, however, is often exorbitantly time consuming, especially when the treatment of the full six-degree-of-freedom seakeeping problem is necessary—namely conditions where nonlinear coupling between the vessel responses leads to a loss of stability (e.g. parametric rolling, broaching).

1.2 Overview

We introduce a new methodology to study the six-degree-of-freedom nonlinear ship motion and stability problem, including strong mode-coupling, extendable to any relevant vessel geometry. It draws upon recent advances in the nonlinear hydrodynamic modeling of the (forward-speed) ship seakeeping problem, introduces a state-space representation of the radiation and diffraction memory effects, and represents the ambient seastate as a state-space-diffusion process conforming to a prescribed spectrum and probability density function. This framework leads to a multi-dimensional stochastic differential equation, and its associated Fokker-Planck equation governing the joint-probability density function of the nonlinear ship motions. This enables the

efficient derivation of the Safe Operating Envelope of the ship in various seastates, speeds and headings.

The time-dependence of the wetted hull gives rise to potential flow nonlinearities in the (forward-speed) ship seakeeping problem, responsible for the strong nonlinear hydrostatic restoring and Froude-Krylov forces. A new formulation of these nonlinear effects was recently introduced by the Fluid Impulse Theory (FIT) derived by Sclavounos [7]. We then derive new expressions for the hydrostatic and Froude-Krylov forces, readily evaluated using the instantaneous ship wetted surface given the ambient wave profile. The radiation and diffraction hydrodynamic disturbances in FIT are computed by three-dimensional time-domain Rankine panel methods. We are able to convert the time-convolution memory integrals of the radiation and diffraction disturbances from the panel method solutions into state-space form by invoking the ESPRIT algorithm, which allows for the respective impulse response functions to be represented by a series of complex exponentials.

Finally, representing the hydrodynamic impulse response functions and ambient seastate in state-space form leads to the conversion of the conventional six-degree-of-freedom equations of motion into a multi-dimensional stochastic differential equation (SDE) for the states governing the nonlinear ship seakeeping problem. The benefit of this stochastic state-space representation is that the joint probability density of the states is governed by a deterministic Fokker-Planck partial differential equation (FPE). The associated FPE may be solved using either Monte-Carlo methods via time-marching ensembles of the SDE, or a recently-developed Galerkin procedure for FPEs of high-dimensionality.

The state-space form may lead to a more straightforward, and faster, deterministic simulation compared to traditional approaches to the nonlinear seakeeping problem, which requires fine discretization of large spatial domains. Additionally,

resulting knowledge of the joint probability density of the states via the FPE may circumvent the need for time consuming Monte Carlo simulations and leads to the direct derivation of criteria governing the ship Safe Operating Envelope.

Chapter 2

Theory Background

In this section, we introduce the background theory and starting point for our work in developing the novel methodology presented herein.

2.1 Fluid Impulse Theory

Our model draws on recent developments in marine hydrodynamics, particularly the introduction of Fluid Impulse Theory (FIT) by Sclavounos in 2012 [7]. We begin by setting up the physical picture and reference coordinate systems.

Consider a free-floating vessel interacting with an ambient wave, illustrated in Figure 2-1. The earth-fixed coordinate system $\boldsymbol{X}$ has its origin centered on the mean-free-surface and at mid-ships. The body-fixed coordinate system $\boldsymbol{\xi}$ initially coincides with the earth-fixed coordinate system in calm water, and remains fixed to the body. An inward-pointing unit normal vector $\boldsymbol{n}$ is defined on the body and dashed incident-wave free surface $\zeta_I(\boldsymbol{X}, t)$, while the unit normal $\boldsymbol{n}_T$ on the total nonlinear wave $\zeta_T(\boldsymbol{X}, t)$ is defined to be pointing outward (up), as shown in Figure

2-1. Gravity points downward, with magnitude $g = 9.81$ [m/s^2].

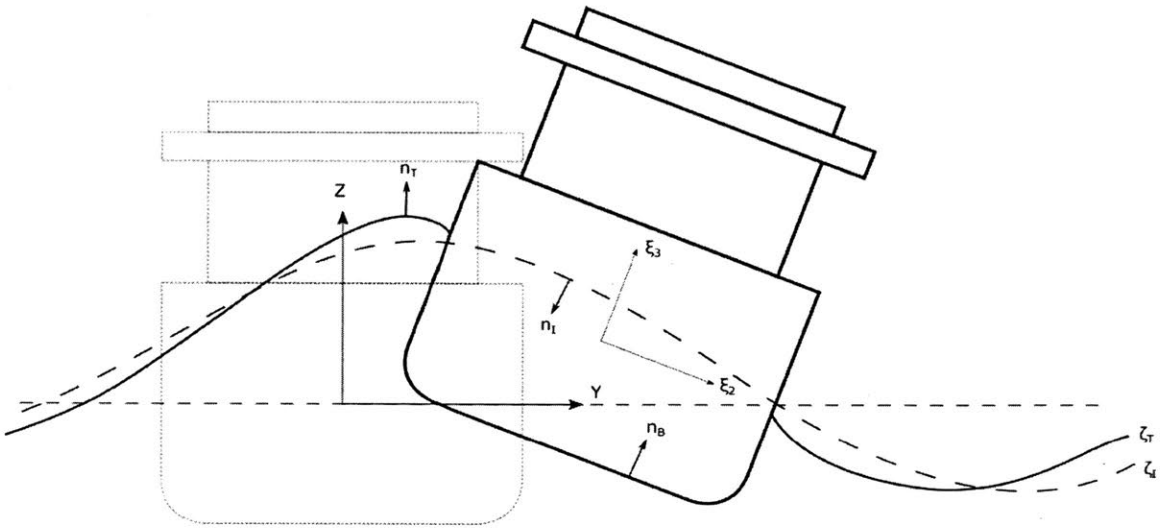

Figure 2-1: A free floating ship in an irregular seastate, with an earth-fixed coordinate system initially located on the mean free surface at mid-ships in calm water. The ambient irregular wave surface is denoted by the dashed line, and the total free surface including body radiation and diffraction disturbances is denoted by the solid line.

Assume the wave fluid flow is represented by an inviscid, incompressible and irrotational flow with density ρ. Under these assumptions, define velocity components $\vec{v}$ as the gradient of a scalar velocity potential ϕ. Additionally, denote the incident ambient and disturbance velocity potentials by $\phi_I(\boldsymbol{X}, t)$ and $\phi_D(\boldsymbol{X}, t)$, respectively. The total velocity potential, $\phi = \phi_I + \phi_D$, satisfies conservation of mass, which reduces to the Laplace equation, in the fluid domain,

$$\frac{\partial^2 \phi}{\partial X^2} + \frac{\partial^2 \phi}{\partial Y^2} + \frac{\partial^2 \phi}{\partial Z^2} = 0 \,. \tag{2.1}$$

The velocity potential must also satisfy the body boundary condition on the wetted

body surface $S_B(t)$

$$\frac{\partial \phi}{\partial n} = U_n \quad \text{on } S_B(t) \ , \tag{2.2}$$

where U_n is the body normal velocity. A free-surface boundary condition, i.e. no fluid flux across the free-surface, is also required.

Assume the ambient wave free surface and corresponding potentials are known a priori and are of $\mathcal{O}(1)$. In this work, we will restrict ourselves to consider only vessels operating in severe stationary stochastic seastates. The disturbance potential corresponds to a vessel disturbance of $\mathcal{O}(\delta), \delta \ll 1$—typically true in long waves experienced in severe design seastate spectra [7]. This permits the use of the weak-scatterer kinematic and dynamic free surface conditions, where the disturbances due to the presence of the body are linearized about the nonlinear ambient wave surface $\zeta_I(\boldsymbol{X}, t)$,

$$\begin{aligned} &\frac{\partial \phi_D}{\partial t} + g\zeta_D + \nabla\phi_D \cdot \nabla\phi_I \\ &\quad - \zeta \frac{\partial}{\partial Z}\left[\frac{\partial \phi_I}{\partial t} + \frac{1}{2}\nabla\phi_I \cdot \nabla\phi_I\right] = 0, \quad Z = \zeta_I(\boldsymbol{X}, t) \end{aligned} \tag{2.3a}$$

$$\begin{aligned} &\frac{\partial \zeta_D}{\partial t} - \frac{\partial \phi_D}{\partial Z} + \nabla\phi_I \cdot \nabla\zeta_D + \nabla\zeta_I \cdot \nabla\phi_D \\ &\quad - \zeta_D\left[\frac{\partial^2 \phi_I}{\partial Z^2} - \nabla\zeta_I \cdot \nabla\left(\frac{\partial \phi_I}{\partial Z}\right)\right] = 0, \quad Z = \zeta_I(\boldsymbol{X}, t) \end{aligned} \tag{2.3b}$$

With knowledge of ϕ_I and ϕ_D, the hydrodynamic forces and moments acting on a vessel with either zero or finite forward speed can be expressed as the time derivative of corresponding impulses [7]. The impulses, in turn, are expressed in terms of

integrals of the corresponding velocity potentials integrated over the instantaneous wetted body surface and projection of the incident wave surface through the body. Hydrostatic forces and moments are similarly expressed in terms of integrals over the instantaneous body volume under the instantaneous ambient wave profile.

From the fluid forces $\boldsymbol{F}$ and moments $\boldsymbol{M}$, calculated in the earth-fixed coordinate frame, the nonlinear equations of motion follow from Newton's law. For this present work, we consider small amplitude response motions, permitting the linearization of Newton's laws, whereby the global coordinate system $\boldsymbol{X}$ and the body-fixed coordinate system $\boldsymbol{\xi}$ are coincident, resulting in

$$m\ddot{\boldsymbol{X}} \approx m\ddot{\boldsymbol{\xi}}_{1,2,3} = \sum \boldsymbol{F} \tag{2.4a}$$

$$\frac{d}{dt}\boldsymbol{L} \approx \boldsymbol{I}\ddot{\boldsymbol{\xi}}_{3,4,5} = \sum \boldsymbol{M} \tag{2.4b}$$

$\boldsymbol{L}$ is the angular momentum vector about the earth-fixed coordinate system in the equations above, and $\boldsymbol{I}$ is the moment of inertia matrix about the body-fixed axes. This simplification is for clarity in the present work, as large-displacement motions are readily-handled by the well-established machinery of state-space and Euler-angle representations. We will now expand on the fluid force compoments.

2.1.1 Nonlinear Froude-Krylov & Hydrostatics

Expressing the Froude-Krylov force and moment in terms of the incident potential ϕ_I, at this point assumed known everywhere in the fluid domain,

$$\boldsymbol{F}_{\text{F-K}}(t) = -\rho\frac{d}{dt}\left[\int\limits_{S_B^w(t)} \phi_I \boldsymbol{n}\, ds + \int\limits_{S_I^w(t)} \phi_I \boldsymbol{n}\, ds\right] \tag{2.5}$$

$$\boldsymbol{M}_{\text{F-K}}(t) =$$
$$-\rho\frac{d}{dt}\left[\int\limits_{S_B^w(t)}\phi_I\left(\boldsymbol{X}\times\boldsymbol{n}\right)\,ds+\int\limits_{S_I^w(t)}\phi_I\left(\boldsymbol{X}\times\boldsymbol{n}\right)\,ds\right]. \tag{2.6}$$

Integrating the incident potential ϕ_I over the instantaneous wetted body surface $S_B^w(t)$ and the instantaneous intersection of the incident wave profile $S_I^w(t)$ with the body, forms a closed surface.

Similarly expressing the nonlinear hydrostatic force and moment as integrals over the closed volume, bounded by the ambient wave profile and the body wetted surface, with an inward-pointing unit normal,

$$\boldsymbol{F}_{\text{B}}(t) = -\rho g\left[\int\limits_{S_B^w(t)}Z\boldsymbol{n}\,ds+\int\limits_{S_I^w(t)}Z\boldsymbol{n}\,ds\right]=\rho g\forall_w(t)\,\boldsymbol{k} \tag{2.7}$$

$$\boldsymbol{M}_{\text{B}}(t) =$$
$$-\rho g\left[\int\limits_{S_B^w(t)}Z\left(\boldsymbol{X}\times\boldsymbol{n}\right)\,ds+\int\limits_{S_I^w(t)}Z\left(\boldsymbol{X}\times\boldsymbol{n}\right)\,ds\right]. \tag{2.8}$$

Necessarily, the hydrostatic force points in vertical $\boldsymbol{k}$ direction, extending the principle of Archimedean hydrostatics,

$$\boldsymbol{F}_{\text{HS}}=\rho g\forall_{\Delta w}\left(\boldsymbol{X},\zeta(t)\right)\boldsymbol{k}\,, \tag{2.9}$$

When considering small displacements, equation 2.9 reduces to the familiar linear hydrostatic restoring term.

The Froude-Krylov and Hydrostatic fluid forces contain strong nonlinearities, which we will address subsequently. For compactness, the remainder of this work discusses only an illustrative force or moment expression at each step. The corresponding moment or force follows in an analogous manner, respectively.

2.1.2 Radiation & Diffraction Disturbances

Similarly expressing the hydrodynamic disturbance force as an integral of the disturbance potential ϕ_D over the instantaneous body wetted surface,

$$\boldsymbol{F}_D(t) = -\rho \frac{d}{dt} \left[\int_{S_B^w(t)} \phi_D \boldsymbol{n} \, ds \right] . \tag{2.10}$$

As the total disturbance potential is $\phi_D = \phi_{\text{Rad}} + \phi_{\text{Diff}}$, The total disturbance force (2.10) is expanded into the radiation and diffraction components,

$$\boldsymbol{F}_{\text{Rad}} = -\rho \frac{d}{dt} \left[\int_{S_B^w(t)} \phi_{\text{Rad}} \boldsymbol{n} \, ds \right] \tag{2.11}$$

$$\boldsymbol{F}_{\text{Diff}} = -\rho \frac{d}{dt} \left[\int_{S_B^w(t)} \phi_{\text{Diff}} \boldsymbol{n} \, ds \right] . \tag{2.12}$$

Note that the disturbance potential will include forward speed effects, when applicable.

2.2 Stochastic Differential Equations

Changing gears, we will now briefly introduce the concept of stochastic differential equations (SDEs) in the context of this work. The stochastic calculus results formulated herein are presented in an implementable form; for further derivations and theory, kindly see the referred works.

Let X_t be the solution of the differential equation for a "noisy" physical process,

$$\frac{dX_t}{dt} = \mu\left(t, X_t\right) + \sigma\left(t, X_t\right)\ B_t \tag{2.13}$$

where B_t is a stochastic "noise" term. Adding a clarifying interjection on notation, the capital variable X or vector $\boldsymbol{X}$ refers to the earth-fixed coordinate system. The capital variable X_t or vector $\boldsymbol{X}_t$ refers to a stochastic process, with the distinguishing subscript. Formally, X_t is the stochastic integral process that satisfies the noisy ODE (2.13) [8]. Stochastic integrals have particular properties that extend and reach, sometimes unintuitively, beyond the realm of traditional deterministic calculus. These stochastic integrals and differential equations (SDEs) for the solution paths of these processes can be defined in several non-unique ways. The most common definition is the Itô stochastic differential equation, which has the general form

$$dX_t = \mu\left(t, X_t\right) dt + \sigma\left(t, X_t\right) dW_t\ . \tag{2.14}$$

dW_t is a unit white noise process, otherwise known as the increments of a unit Wiener process (the Wiener process is also known as the "standard Brownian motion" to some authors). When $\sigma(t, X_t)$ does not exhibit any memory, then the process X_t described by either (2.14) or (2.16) is called a "diffusion" process. In other words,

the process X_t obeys the Markov property [8],

$$\text{Prob}\left(X_n = x_n | X_{n-1} = x_{n-1}, \ldots, X_1 = x_1\right) = \text{Prob}\left(X_n = x_n | X_{n-1} = x_{n-1}\right) \quad (2.15)$$

As mentioned, there are several alternative definitions of stochastic integrals to (2.14). One in particular, the Stratonovich form [9], is important to the framework presented herein,

$$dX_t = \mu\left(t, X_t\right) dt + \sigma\left(t, X_t\right) \circ dW_t \; . \quad (2.16)$$

The $\circ$ symbol denotes a Stratonovich integral. In general, computing the solutions of (2.14) and (2.16) for the same μ and σ lead to different answers.

This leads to the question: what is the difference between the two forms, and which one should we use? Comparing and contrasting them, the Itô form lends an easier numerical simulation of the process X_t, but differentiation of scalar functions of the process X_t is cumbersome, requiring the application of Itô's Lemma (the stochastic extension of the ordinary chain rule). The Stratonovich form, on the other hand, has two beneficial and necessary properties. First, it is defined such that applying Itô's Lemma appears as the ordinary calculus chain rule—the higher order terms cancel. Second, as shown by Wong and Zakai, for many physical processes, the Stratonovich integral gives the correct solution of X_t to the corresponding SDE, while the Itô integral does not [10]. Simply, this occurs because, in general, the diffusion coefficients of many physical processes are not constant over the stochastic increment. However, for any Itô integral, there exists a corresponding Stratonovich integral. This different solution to what superficially appears to be the same SDE is a

subtle but important point for working with stochastic calculus. However, by choosing the Stratonovich form, the reader is not required to go significantly further in order to understand the practical formulation and implementation of the framework that follows. Lastly, the process X_t may be a scalar or multi-dimensional process [8, 9]. Please refer to Appendix A for more details on Stochastic integration, and for a more complete introduction to the theory that extends beyond the practical implementation of this work, Øksendal (2010).

But why introduce this more complex and obscure way of modeling the physical process? We do so to sidestep running computationally-expensive Monte-Carlo simulations for the response probability distributions. Instead, we can get the same information from another approach.

2.2.1 The Fokker-Planck Equation

We introduce the Fokker-Planck equation (FPE), also known as the Komogorov-Forward-Equation [11, 12, 8, 13]. It governs the time-evolution of the joint probability density function (PDF) of the states of the multidimensional stochastic diffusion process, $\boldsymbol{X}_t$ that satisfies either form SDE, (2.14) or (2.16). It may be solved for the stationary case where the left-hand-side of (2.17) is zero, or the transient case where it is non-zero.

The FPE for the general Stratonovich SDE (5.16) is the deterministic partial differential equation [13],

$$\frac{\partial p(\boldsymbol{x},t)}{\partial t} = -\sum_{i=1}^{N} \frac{\partial}{\partial x_i}\left[\mu_i(\boldsymbol{x},t)\, p(\boldsymbol{x},t)\right] + \frac{1}{2}\sum_{k=1}^{M}\sum_{i=1}^{N} \frac{\partial}{\partial x_i}\left\{\sigma_{ik}(\boldsymbol{x},t)\sum_{j=1}^{N}\frac{\partial}{\partial x_j}\left[\sigma_{jk}(\boldsymbol{x},t)\, p(\boldsymbol{x},t)\right]\right\}. \tag{2.17}$$

We make the distinction here between the deterministic dummy variables x_i and $\boldsymbol{x}$ in the FPE and the stochastic state variable $x_{t,i} \in \boldsymbol{X}_t$, used in (5.16).

By solving the FPE for the joint PDF of (5.16), we can analyze it with respect to the seakeeping states, particularly the motion states. This result paints the complete picture, with all necessary information, of the stability analysis, including traditional stability measures such as level crossing rates. Additionally, heavy tails or breakdown in the FPE solution are indicative of more severe or singular behavior. Thus from this PDF, we can determine the SOE in a given seastate, easily extending to a family of seastates. The major advantage offered by this method is that all the necessary information follows from solving the FPE only once for a prescribed design seastate, rather than requiring many Monte-Carlo runs simulating the vessel responses to achieve convergent average results.

Chapter 3

Seakeeping Hydrodynamics

We will now expand the FIT fluid force terms introduced in Section 2.1 into a more accessible form.

3.1 Linearized Disturbances

By virtue of the assumption of small body wave disturbances, we linearize the radiation and diffraction forces about the incident wave profile. Invoking the weak-scatterer hypothesis, the ship motions are allowed to be large and assumed comparable to the wave amplitude, while the radiation/diffraction disturbances are assumed small.

Treating the radiation component by considering an oscillating body, and linearizing about the mean position of the free surface and body surface, the linear radiation force is represented in the standard Cummins impulse-response form in the body-fixed coordinate system,

$$F_{i,\mathrm{Rad}}(t) = A_{ij,\infty}\,\ddot{\xi}_j + \int_0^t k_{ij,\mathrm{Rad}}(t-\tau)\,\dot{\xi}_j(\tau)\;d\tau\;. \tag{3.1}$$

The radiation impulse response kernel $k_{\mathrm{Rad}}(\tau)$ is causal, and the system is assumed to start from zero-initial conditions at $t = 0$.

We similarly linearize the diffraction component and represent it by an analogous impulse response convolution,

$$F_{i,\mathrm{Diff}}(t) = \int_{-\infty}^{t+t_{c,\mathrm{Diff}}} k_{i,\mathrm{Diff}}(t-\tau)\,\zeta_I(\tau)\;d\tau\;. \tag{3.2}$$

Note the linear diffraction component is expressed in terms of the incident wave elevation $\zeta_I(t)$, measured at the origin. Unlike the linear radiation component, the linear diffraction impulse kernel is non-causal, with a finite non-causal convolution horizon $t_{c,\mathrm{Diff}}$, as explained by Yu and Falnes [14]. These two linear components, radiation and diffraction, contain the wave memory effects of the system. To reduce clutter, we drop the spatial location, and subsequent uses of ζ_I are implied to be measured at the origin, unless otherwise noted.

Similarly expanding the Froude-Krylov component into a linear and nonlinear term, with respect to the wetted body surface,

$$F_{i,\text{F-K}}(t) = \int_{-\infty}^{t+t_{c,\text{FK}}} k_{i,\text{F-K}}(t-\tau)\,\zeta_I(\tau)\;d\tau$$
$$- \rho\frac{d}{dt}\left[\int_{\Delta S^w(t)} \phi_I n_i\; ds\right] . \tag{3.3}$$

The linear Froude-Krylov impulse kernel is also non-causal with a finite convolution horizon $t_{c,\text{FK}}$. We will now take $t_c \equiv \max(t_{c,\text{Diff}}, t_{c,\text{FK}})$. The nonlinear Froude-Krylov component is now integrated over the instantaneous differential surface formed by the incident wave surface inside the body, the calm water waterplane area and the differential wetted surface around the waterline, $\Delta S^w(t) = \Delta\left[S_B^w(t) - S_{B,0}^w + S_I^w(t)\right]$. Figure 3-1 illustrates the differential surface $\Delta S^w(t)$ as the bold boundary surrounding the shaded red differential volume.

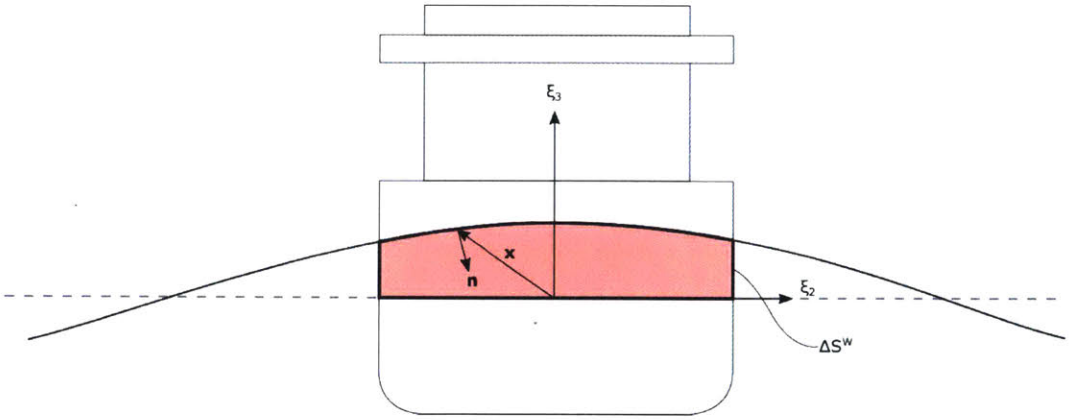

Figure 3-1: The closed differential surface, $\Delta S^w(t)$ denoted by the bold boundary around the corresponding differential volume (shaded red) under the instantaneous intersection of the ambient wave and the body, whose motion has been linearized.

Implicit in this expansion is the assumption that the wetted body beneath the calm

waterline linearly interacts with the incident wave. For continuity in assumptions, a linear ambient seastate potential ϕ_I is required, suggesting the intuitive conclusion that the strong nonlinearities arise from the time-dependent differential wetted body surface $\Delta S^w(t)$. The same is true for the hydrostatic component, which for now will be left as an exact nonlinear function, parameterized by the body displacement and the incident wave elevation,

$$\boldsymbol{F}_{\mathrm{HS}}(t) = \boldsymbol{F}_{\mathrm{HS}}\left(\boldsymbol{\xi}, S_I^w(t) \approx \zeta_I(t)\right) \ . \tag{3.4}$$

Combining the linear Froude-Krylov and diffraction components into a single excitation component, the conventional right-hand-side of the linear seakeeping equations of motion takes shape,

$$\begin{aligned} F_{i,\mathrm{Ex}}(t) &= F_{i,\mathrm{Diff}}(t) + F_{i,\text{F-K,linear}}(t) \\ &= \int_{-\infty}^{t+t_c} k_{i,\mathrm{Ex}}(t-\tau)\,\zeta_I(t)\ d\tau \\ &= \int_{-\infty}^{t} k_{i,\mathrm{Ex}}(t-\tau)\,\zeta_I(t)\ d\tau \\ &+ \int_{t}^{t+t_c} k_{i,\mathrm{Ex}}(t-\tau)\,\zeta_I(t)\ d\tau \ , \end{aligned} \tag{3.5}$$

where $k_{i,\mathrm{Ex}} = k_{i,\text{F-K}} + k_{i,\mathrm{Diff}}$. In anticipation of the formulation of the stochastic model in Section 4, the limits of integration are split in the final line of (3.5) into causal and non-causal integrals.

Evaluating the linear excitation only requires knowledge of the incident wave

elevation at the origin. Evaluating the nonlinear Froude-Krylov component, however, requires knowledge of the instantaneous differential wetted surface and the incident velocity potential over that surface. To build anticipation, Section 2.2 will address this challenge.

3.1.1 Computing the Linear Impulse Response Kernels

Before continuing to the nonlinear fluid forces, we complete the model of the linear hydrodynamics by computing the linear excitation and radiation impulse response kernels, $k_{i,\mathrm{Ex}}(\tau)$ and $k_{ij,\mathrm{Rad}}(\tau)$, respectively. These kernels have been used extensively in (linear) seakeeping analysis, and are readily found by employing standard panel method codes.

Our formulation thus far has made no assumption on the absence of forward speed effects. With the inclusion of finite forward speed effects, a time-domain code must be used. In the absence of forward speed, time domain (SWAN) or frequency domain (WAMIT) panel codes may be used to compute the impulse response functions.

For illustrative purposes, we present a frequency-domain formulation using WAMIT, applied to a rectangular barge in beam waves, with particulars summarized in Table 3.1. WAMIT computes the added mass $A(\omega)$ and damping $B(\omega)$ coefficients, and complex linear excitation force $\mathbb{F}(\omega)$ as a function of pre-determined frequencies. Figure 3-2 shows the mesh of the barge used, using 1600 panels, over a quarter-domain, exploiting x-axis and y-axis symmetries to expedite calculations.

Table 3.1: Barge specifications

	Full Vessel
Length [m]	110
Beam [m]	10
Draft [m]	5
End Radius [m]	5

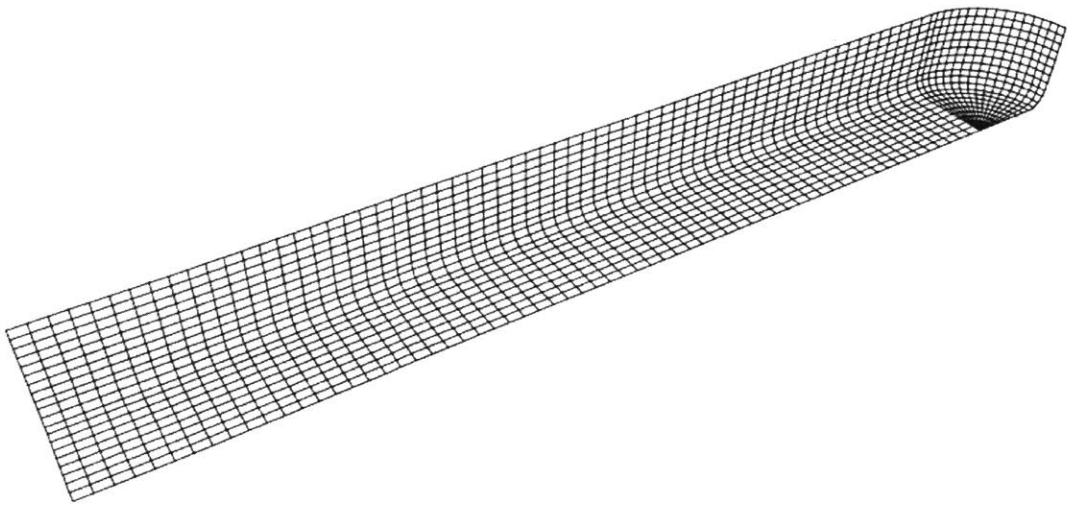

Figure 3-2: Barge surface discretization using 1600 rectangular panels over the quarter-body domain, supplied to WAMIT.

The radiation impulse kernel follows from invoking the Ogilvie relationships [15],

$$A_{ij}(\omega) = A_{ij,\infty} - \frac{1}{\omega}\int_0^\infty k_{ij,\mathrm{Rad}}(\tau)\sin(\omega\tau)\ d\tau \tag{3.6a}$$

$$B_{ij}(\omega) = \int_0^\infty k_{ij,\mathrm{Rad}}(\tau)\cos(\omega\tau)\ d\tau\ . \tag{3.6b}$$

Inverting these relations, the impulse may be computed from either of the following formulae:

$$k_{ij,\mathrm{Rad}} = \frac{1}{2\pi}\int_0^\infty \omega\left[A_{ij,\infty} - A_{ij}(\omega)\right]\sin(\omega\tau)\ d\omega \tag{3.7a}$$

$$k_{ij,\mathrm{Rad}} = \frac{1}{2\pi}\int_0^\infty B_{ij}(\omega)\cos(\omega\tau)\ d\omega\ . \tag{3.7b}$$

Computing k_{Rad} via (3.7b) is more reliable than via (3.7a), as estimating the infinite-frequency added mass $A_{ij,\infty}$ is computationally challenging.

The linear excitation impulse response kernel follows directly from linear system theory, as the inverse Fourier transform of the complex linear excitation force output of WAMIT, $\mathbb{F}_i(\omega)$,

$$k_{i,\mathrm{Ex}}(\tau) = \frac{1}{2\pi}\int_{-\infty}^\infty \mathbb{F}_i(\omega)\, e^{i\omega\tau}\ d\tau\ , \tag{3.8}$$

$\mathbb{F}_i(\omega)$ is the complex force transfer function, whose inverse Fourier transform is real-valued. Figure 3-3 plots the linear roll excitation impulse response kernel in beam waves, and linear roll radiation kernel for the barge.

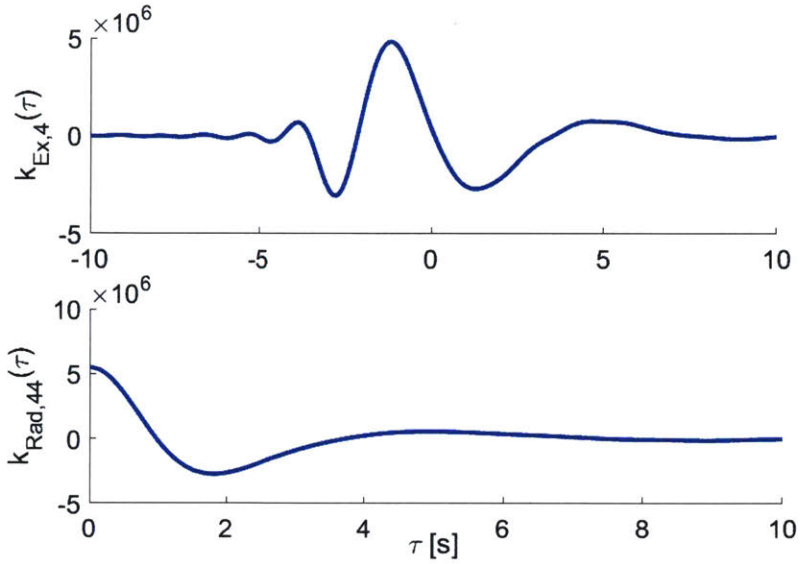

Figure 3-3: Barge linear roll excitation (top) in beam waves and roll radiation (bottom) kernel.

With the complete formulation of the traditional linear seakeeping problem in an impulse-response form, we return to the nonlinear Froude-Krylov and hydrostatic components.

3.2 The Nonlinear Froude-Krylov Model

We treat the nonlinear Froude-Krylov and hydrostatic forces for the restored modes, where Froude-Krylov components are known to dominate diffraction components [7]. Considering the roll-mode for the wall-sided barge described above, the nonlinear Froude-Krylov moment is

$$F_{4,\text{F-K,nl}}(t) = -\rho \frac{d}{dt} \left[\int_{\Delta S_w(t)} \phi_I(\boldsymbol{x}, t)\, (\boldsymbol{x} \times \boldsymbol{n})\, ds \right] . \tag{3.9}$$

Begin simplifying (3.9) by expanding the cross product over the surface $\Delta S_w(t)$. The normal vector $\boldsymbol{n}$ and the position vector $\boldsymbol{x}$ are nearly collinear over the side walls of the barge, so we neglect the integral over those surfaces. The normal vector to the mean free surface is $\boldsymbol{n} = (0, 1)$, and to leading order, the normal vector to the mean free surface is $\boldsymbol{n} = (0, -1)$, simplifying the cross-product term to $(\boldsymbol{x} \times \boldsymbol{n}) = yn_2$.

We can illustrate this claim over the ambient wave profile in a more rigorous manner. Consider the scenario when the ambient wavelength is long compared to the beam of the vessel. The ambient wave projection through the body is approximated by a linear function in y,

$$\zeta_I(y,t) = \eta_I(t)\, y + \zeta_I(t) \tag{3.10}$$

The z-intercept is $\zeta_I(t)$ and the slope is $\eta_I(t)$. Upon the introduction of the stochastic model in Section 4, the slope will also be a stochastic process. For now, if we are considering a deterministic seastate, then the slope $\eta_I(t)$ is also deterministic. The normal vector is expressed exactly in terms of the free surface slope,

$$n_1 = \frac{\eta_I}{\sqrt{1+\eta_I^2}}, \quad n_2 = \frac{-1}{\sqrt{1+\eta_I^2}}\,. \tag{3.11}$$

Therefore, $(\boldsymbol{x} \times \boldsymbol{n})$ over the ambient wave profile reduces to

$$\boldsymbol{x} \times \boldsymbol{n} = -\frac{y\,(1+\eta_I^2) + \eta_I \zeta_I}{\sqrt{1+\eta_I^2}}\,\hat{\boldsymbol{i}}\,. \tag{3.12}$$

Substituting this approximation into (3.9), the integral simplifies,

$$
\begin{aligned}
F_{4,\text{F-K,nl}}(t) &= -\rho\frac{d}{dt}\left[\int\limits_{\Delta S_w(t)} \phi_I(y,z,t)\left\{\frac{y\left(1+\eta_I^2\right)+\eta_I\zeta_I}{\sqrt{1+\eta_I^2}}\right\} ds\right] \\
&= \rho\frac{d}{dt}\left[\int\limits_{S_w(t)} \phi_I(y,z,t)\left\{\frac{y\left(1+\eta_I^2\right)+\eta_I\zeta_I}{\sqrt{1+\eta_I^2}}\right\} ds - \int\limits_{\bar{S}_w} \phi_I(y,0,t)\, y\, ds\right] \\
&= \rho\frac{d}{dt}\int\limits_{\bar{S}_w}\left[\phi_I(y,\zeta_I,t)\sqrt{1+\eta_I^2}-\phi_I(y,0,t)\right] y + \phi_I(y,\zeta_I,t)\frac{\eta_I\zeta_I}{\sqrt{1+\eta_I^2}}\, ds
\end{aligned}
\tag{3.13}
$$

Taking the Taylor expansion of $\sqrt{1+\eta_I^2}$ and $\eta_I/\sqrt{1+\eta_I^2}$ about $\eta_I = 0$,

$$
\sqrt{1+\eta_I^2} = 1 + \frac{\eta_I^2}{2} - \frac{\eta_I^4}{8} + \cdots \tag{3.14a}
$$

$$
\frac{\eta_I}{\sqrt{1+\eta_I^2}} = \eta_I - \frac{\eta_I^3}{2} + \frac{3\eta_I^5}{8} - \cdots \tag{3.14b}
$$

Now substituting in the Taylor expansions to (3.13), rearranging, and retaining up to quadratic terms in the expansions,

$$
\begin{aligned}
F_{4,\text{F-K,nl}}(t) &= \rho\frac{d}{dt}\int\limits_{\bar{S}_w}\left[\phi_I(y,\zeta_I,t)\left[1+\frac{\eta_I^2}{2}\right]-\phi_I(y,0,t)\right] y + \phi_I(y,\zeta_I,t)\left[\zeta_I\eta_I\right]\, ds \\
&= \rho\frac{d}{dt}\int\limits_{\bar{S}_w}\left[\phi_I(y,\zeta_I,t)-\phi_I(y,0,t)\right] y + \phi_I(y,\zeta_I,t)\left[\zeta_I\eta_I + y\frac{\eta_I^2}{2}\right]\, ds
\end{aligned}
\tag{3.15}
$$

Under the assumption of a linear ambient wave, the potential is easy to evaluate at $z = 0$, but is not defined at $z = \zeta_I$, above the mean free surface. Therefore, using a left-endpoint rule approximation to the definition of the (z-partial) derivative, we make the following substitution,

$$
\phi_I(y,\zeta_I,t) - \phi_I(y,0,t) = \frac{\partial\phi_I(y,0,t)}{\partial z}\zeta_I(y,t) \tag{3.16}
$$

$$F_{4,\text{F-K,nl}}(t) = \rho \frac{d}{dt} \int\limits_{\bar{S}_w} \left[\frac{\partial \phi_I(y,0,t)}{\partial z} \zeta_I(y,t) \right] y + \phi_I(y, \zeta_I, t) \left[\zeta_I \eta_I + y \frac{\eta_I^2}{2} \right] \, ds \quad (3.17)$$

To address the remaining $\phi_I(y, \zeta_I, t)$ term, we add and subtract $\phi_I(y,0,t) \left[\zeta_I \eta_I + y \frac{\eta_I^2}{2} \right]$ to perform the same derivative substitution trick on the quadratic terms. The resulting expression for the nonlinear Froude-Krylov moment is

$$\begin{aligned} F_{4,\text{F-K,nl}}(t) = \rho \frac{d}{dt} \int\limits_{\bar{S}_w} & \left[\frac{\partial \phi_I(y,0,t)}{\partial z} \zeta_I(y,t) \right] \left[y \left(1 + \frac{\eta_I^2}{2} \right) + \zeta_I \eta_I \right] \\ & + \phi_I(y,0,t) \left[\zeta_I \eta_I + y \frac{\eta_I^2}{2} \right] \, ds \end{aligned} \quad (3.18)$$

As the integral in (3.18) is expressed over the mean free surface, applying Leibniz's rule simply exchanges the order of differentiation and integration. Making a premonitory remark, caution must be taken when taking the derivative of this function in the context of the stochastic differential equations to be introduced in later sections, when ζ_I and η_I will be stochastic processes.

Returning to the original claim that we may only retain the leading order terms, we see that all multipliers of the potential are of order $\mathcal{O}(0)$ or $\mathcal{O}(2)$. Neglecting higher order terms, and treating the ambient wave as linear, preserving consistency with approximations made thus far, we apply the linear free surface condition,

$$\frac{\partial \phi_I(y,0,t)}{\partial z} = \frac{\partial \zeta_I(y,t)}{\partial t} \quad (3.19)$$

$$F_{4,\text{F-K,nl}}(t) = \rho \frac{d}{dt} \int\limits_{\bar{S}_w} \frac{\partial \zeta_I(y,t)}{\partial t} \zeta_I(y,t) \, y \, ds \quad (3.20)$$

Neglecting higher order terms removes the potential complexity in differentiating the integrand, when it becomes stochastic in the later stages of the framework. Finally,

taking the derivative inside, we arrive at the quadratic nonlinear Froude-Krylov roll moment,

$$F_{4,\text{F-K,nl}}(t) = \rho \int_{\bar{S}_w} \left[\left(\frac{\partial \zeta_I(y,t)}{\partial t} \right)^2 + \frac{\partial^2 \zeta_I(y,t)}{\partial t^2} \zeta_I(y,t) \right] y \, ds \, . \tag{3.21}$$

Under this model, the nonlinear hydrostatic moment follows similarly,

$$F_{4,HS}(t) = \rho g \int_{\bar{S}_w} \zeta_I(y,t) \, y \, dy \tag{3.22}$$

However, we need to choose how we will model the the integrand. Two models are proposed: a Volterra-type deterministic model, and a semi-discrete stochastic model introduced in Section 5.

3.2.1 Volterra-Type Representation

To compute the nonlinear fluid forces, we desire to model the incident potential at any field point $\boldsymbol{x}$ in the fluid domain in terms of the incident wave elevation measured at the origin. The following Volterra-kernel representation is reserved for deterministic calculations at the moment, and subject to further study. We can introduce the incident velocity potential as the convolution integral

$$\phi_I(\boldsymbol{x},t) = \int_{-\infty}^{\infty} k_\phi(\boldsymbol{x}, t-\tau) \, \zeta_I(\tau) \; d\tau \, . \tag{3.23}$$

Bingham gives the kernel k_ϕ in (3.23) for a linear wave velocity potential with heading β in the integral form [16],

$$k_\phi(\boldsymbol{x},\tau) = \Re\{\mathbb{K}_\phi(\boldsymbol{x},\tau)\} =$$
$$\Re\left\{\frac{g}{\pi}\int_{-\infty}^{\infty}\frac{i}{\omega}\exp\left[kz + i\left(\omega\tau - kx\cos\beta - ky\sin\beta\right)\right]\,d\omega\right\}. \tag{3.24}$$

Substituting (3.23) into (3.18), we can express the nonlinear Froude-Krylov component in terms of the incident wave elevation measured at the origin.

We have found the kernel integral admits a convenient closed form in beam waves, $\beta = \pi/2$, in terms of the complex error function. Define

$$\epsilon \equiv \frac{-z + ix}{g}. \tag{3.25}$$

Taking the time-derivative of the complex kernel $\mathbb{K}_\phi$ and substituting in ϵ, we can manipulate the resulting integral,

$$\begin{aligned}
&-\frac{g}{2\pi}\int_{-\infty}^{\infty}\exp\left[-\left(\epsilon\omega^2 - i\omega t\right)\right]\,d\omega \\
&= -\frac{g}{2\pi}\left[\int_{-\infty}^{0}\exp\left[-\left(\epsilon\omega^2 - i\omega t\right)\right]\,d\omega + \int_{0}^{\infty}\exp\left[-\left(\epsilon\omega^2 - i\omega t\right)\right]\,d\omega\right] \qquad (3.26)\\
&= -\frac{g}{2\pi}\left[-\int_{0}^{-\infty}\exp\left[-\left(\epsilon\omega^2 - i\omega t\right)\right]\,d\omega + \int_{0}^{\infty}\exp\left[-\left(\epsilon\omega^2 - i\omega t\right)\right]\,d\omega\right]
\end{aligned}$$

Let $u = -\omega$ in the first integral,

$$= -\frac{g}{2\pi}\left[\int_{0}^{\infty}\exp\left[-\left(\epsilon u^2 + iut\right)\right]\,du + \int_{0}^{\infty}\exp\left[-\left(\epsilon\omega^2 - i\omega t\right)\right]\,d\omega\right] \tag{3.27}$$

Re-defining $u = \omega$,

$$= -\frac{g}{2\pi} \int_0^\infty 2\cos(\omega t) \exp\left(-\epsilon\omega^2\right)\, d\omega \tag{3.28}$$

Taking the anti-derivative under the integral sign retrieves the original kernel, which now reduces to

$$k_\phi(y,z,\tau) = \Re\left\{ \int_0^\infty \tau \mathrm{sinc}(\tau\omega) \exp\left(-\epsilon\omega^2\right)\, d\omega \right\} . \tag{3.29}$$

For $\Re\{\epsilon\} > 0$, the integral has the closed form,

$$k_\phi(y,z,\tau) = \Re\left\{ -\frac{g}{2}\mathrm{erf}\left(\frac{\tau}{2\sqrt{\epsilon}}\right) \right\} . \tag{3.30}$$

This form is only valid at the calm water free surface and below, however this restriction on the domain is indeed consistent with the linear-wave approximation made so far.

Recalling (3.18), we substitute in (3.23). Omitting the higher order terms and bringing the time derivative inside the integral,

$$\begin{aligned} &F_{4,\text{F-K,nl}}(t) \\ &= \rho \int_{\bar{S}_w} \frac{d}{dt}\left[\frac{\partial\phi_I(y,0,t)}{\partial z}\zeta_I(y,t)\right] y\, ds \\ &= \rho \int_{\bar{S}_w} \frac{d}{dt}\left\{ \left[\frac{\partial}{\partial z}\int_{-\infty}^{\infty} k_\phi(\boldsymbol{x}, t-\tau)\,\zeta_I(\tau)\, d\tau\right]\left[-\frac{1}{g}\frac{\partial}{\partial t}\int_{-\infty}^{\infty} k_\phi(\boldsymbol{x}, t-\tau)\,\zeta_I(\tau)\, d\tau\,.\right]\right\} y ds \end{aligned} \tag{3.31}$$

As z is not a variable of integration in the first integral, take the derivative under the integral sign in the first inner integral. As the limits of the convolutions are not functions of t, also take the partial time derivative in the second inner integral under the integral sign. These modified kernels are,

$$k_{\phi_z}(\boldsymbol{x},\tau) = \Re\left\{-\frac{\tau}{4\epsilon\sqrt{\pi\epsilon}}\exp\left[-\left(\frac{\tau}{2\sqrt{\epsilon}}\right)^2\right]\right\} \tag{3.32a}$$

$$k_{\zeta}(\boldsymbol{x},\tau) = \Re\left\{-\frac{-g}{2\sqrt{\pi\epsilon}}\exp\left[-\left(\frac{\tau}{2\sqrt{\epsilon}}\right)^2\right]\right\} \tag{3.32b}$$

Substituting in the modified kernels, we note that the dummy integration variables τ in the two inner integrals are not the same dummy variable.

$$F_{4,\text{F-K,nl}}(t) = -\frac{\rho}{g}\int_{\bar{S}_w}\frac{d}{dt}\left\{\left[\int_{-\infty}^{\infty} k_{\phi_z}(\boldsymbol{x},t-\tau)\,\zeta_I(\tau)\;d\tau\right]\left[\int_{-\infty}^{\infty} k_{\zeta}(\boldsymbol{x},t-\tau)\,\zeta_I(\tau)\;d\tau\,.\right]\right\} y\,ds \tag{3.33}$$

By regrouping the inner integrals as a double integral, the construct above is in fact, the second order Volterra kernel for the Froude-Krylov force over an infinitesimal slice of the beam, with respect to the ambient wave elevation measured at the origin,

$$\begin{aligned} F_{4,\text{F-K,nl}}(t) &= -\frac{\rho}{g}\int_{\bar{S}_w}\frac{d}{dt}\left\{\int_{-\infty}^{\infty}\int_{-\infty}^{\infty} k_{\phi_z}(\boldsymbol{x},t-\tau_1)\,k_{\zeta}(\boldsymbol{x},t-\tau_2)\,\zeta_I(\tau_1)\,\zeta_I(\tau_2)\;d\tau_1 d\tau_2\right\} y\,ds \\ &= -\frac{\rho}{g}\int_{\bar{S}_w}\left\{\int_{-\infty}^{\infty}\int_{-\infty}^{\infty} k_{\phi,2}(y,t-\tau_1,t-\tau_2)\,\zeta_I(\tau_1)\,\zeta_I(\tau_2)\;d\tau_1 d\tau_2\right\} y\,ds \end{aligned} \tag{3.34}$$

$$\begin{aligned} k_{\phi,2}(\boldsymbol{x},\tau_1,\tau_2) = \Re\Bigg\{&-\frac{1}{4\epsilon\sqrt{\pi\epsilon}}\exp\left[-\left(\frac{\tau_1}{2\sqrt{\epsilon}}\right)^2\right] \\ &+\frac{\tau_1^2}{8\epsilon^2\sqrt{\pi\epsilon}}\exp\left[-\left(\frac{\tau_1}{2\sqrt{\epsilon}}\right)^2\right]\Bigg\}\Re\left\{-\frac{-g}{2\sqrt{\pi\epsilon}}\exp\left[-\left(\frac{\tau_2}{2\sqrt{\epsilon}}\right)^2\right]\right\} \\ &+\Re\left\{-\frac{\tau_1}{4\epsilon\sqrt{\pi\epsilon}}\exp\left[-\left(\frac{\tau_1}{2\sqrt{\epsilon}}\right)^2\right]\right\}\Re\left\{\frac{-g\tau_2}{4\epsilon\sqrt{\pi\epsilon}}\exp\left[-\left(\frac{\tau_2}{2\sqrt{\epsilon}}\right)^2\right]\right\} \end{aligned} \tag{3.35}$$

As a final remark on this representation, note that, although we assumed beam waves, for the sole purpose of setting the wave heading $\beta = \pi/2$, the present formulation is not restricted to beam waves. Any heading β may be used with this form, simply by performing a local coordinate transform for ϵ used in (3.35). The transform is simply a planar rotation about the z-axis, and as the kernel is computed a priori to any simulation, need not be done online during time-marching.

3.3 Equations of Motion

We conclude this section by assembling the (small displacement) equations of motion in the familiar coupled ODE for the i^{th}-mode in the body-fixed coordinate system, using either choice of the nonlinear Froude-Krylov moment, (3.21) or (3.34),

$$\left(m_{ij} + A_{ij,\infty}\right) \ddot{\xi}_j + \int_0^t k_{ij,\text{Rad}}(t-\tau)\dot{\xi}_j(\tau)\, d\tau + \rho g \forall_\Delta \left(\boldsymbol{\xi}, \zeta_I\left(t\right)\right) \boldsymbol{k} = \int_0^{t+t_c} k_{ij,\text{ex}}(t-\tau)\zeta_I(\tau)\, d\tau + F_{i,\text{F-K,nl}}\left(t\right) \tag{3.36}$$

We will now assume the nonlinear Froude-Krylov moment to have the form (3.21) to be used in the stochastic model in Section 5. Note the nonlinear inertia terms in Newton's law have been omitted for clarity.

Chapter 4

The State-Space Formulation

The nature and properties of the stochastic model to follow motivates us to re-cast the equations of motion into state-space form. However, even for deterministic simulations, it has significant advantages, whereby it eliminates the need for evaluating convolutions when simulating the response to deterministic seastates (or seastates known a priori). The following procedure converts the linear components into a linear state-space form comprised of a finite number of hidden states containing the wave memory and convolution effects. The hydrostatics and Froude-Krylov components will remain nonlinear.

4.1 The ESPRIT Algorithm

We may approximate the kernel $k(\tau)$ by a finite sum of N complex exponentials and complex coefficients with arbitrarily sufficient accuracy for positive time,

$$k(\tau) = \sum_{n=1}^{N} c_n \exp[\beta_n \tau] \quad \tau \geq 0; \quad c, \beta \in \mathbb{C} \,. \tag{4.1}$$

To find the exponentials β_n and coefficients c_n, we employ the ESPRIT (Estimation of Signal Parameters via Rotational Invariance Techniques) algorithm [17]. Under ESPRIT, the complex parameters c_n and β_n in (4.1) appear as complex-conjugate pairs, yielding a real-valued approximation to the function $k(\tau)$. ESPRIT has an optimal parameter combination to be selected for each kernel in order to achieve a satisfactory fit with the minimal N number of terms. See Casanovas [18] for more detail.

We are able to fit the linear radiation impulse response kernel directly, as it is causal, resulting in the corresponding coefficients c_{R} and β_{R},

$$k_{\mathrm{Rad}}(\tau) = \sum_{n=1}^{N_{\mathrm{R}}} c_{n,\mathrm{R}} \exp\left[\beta_{n,\mathrm{R}}\tau\right] \ . \tag{4.2}$$

This is carried out for each relevant mode of motion and cross-coupled kernel to the problem of interest. Figure 4-1 illustrates the excellent accuracy of the ESPRIT fit with a small number of terms ($N = 4$) for the barge radiation impulse kernel presented in Figure 3-3.

A more delicate treatment is required for the non-causality present in the excitation impulse response kernels. We are initially tempted to shift the kernel by $-t_c$, making it causal in the shifted coordinate, and then apply ESPRIT. However, recalling the convolution integral has been split into causal and non-causal parts in (3.5), our alternative approach is to fit a two-sided kernel for each half integral. This approach is motivated by anticipating a separate treatment of the wave excitation causal and non-causal components in the stochastic model to follow.

Hence, we fit the causal component of the linear excitation impulse kernel in an

identical manner to the radiation impulse kernel,

$$k_{\mathrm{Ex,causal}}(\tau) = \sum_{n=1}^{N_{\mathrm{Ex}}} c_{n,\mathrm{Ex}} \exp\left[\beta_{n,\mathrm{Ex}}\tau\right]; \quad \tau \geq 0\,. \tag{4.3}$$

The kernel $k_{\mathrm{Ex,causal}}(\tau)$ is identically the right half of $k_{i,\mathrm{Ex}}(\tau)$ $\tau \geq 0$ for positive time. The coefficients for the causal linear excitation force are denoted c_{Ex} and β_{Ex}. Figure 4-1 also illustrates a fit with $N = 4$ ESPRIT terms.

The purely non-causal component of the kernel may be fit by ESPRIT by taking the opposite sign of time τ,

$$k_{\mathrm{Ex,noncausal}}(\tau) = \sum_{n=1}^{N_{\mathrm{Ex,nc}}} c_{n,\mathrm{Ex,nc}} \exp\left[-\beta_{n,\mathrm{Ex,nc}}\tau\right]; \quad \tau \leq 0\,. \tag{4.4}$$

However, we will see that the non-causal ESPRIT fit will not be necessary in expressing the excitation forces. Instead $k_{\mathrm{Ex,noncausal}}(\tau)$ $\tau < 0$ will be used directly.

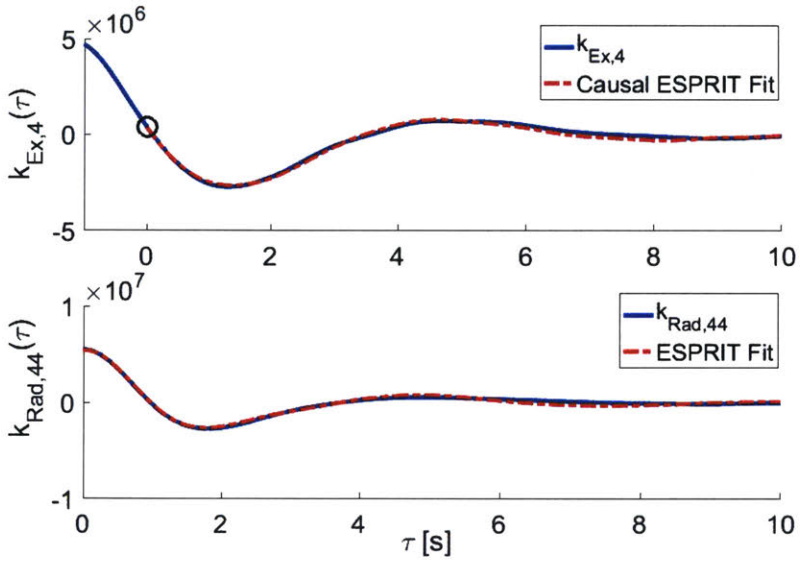

Figure 4-1: ESPRIT fit (red) of the causal excitation (top) and radiation (bottom) impulse kernels compared to the respective WAMIT kernels (blue) for the barge roll motion in beam waves using $N = 4$ terms.

This representation is significant because the fairly arbitrarily-shaped impulse response kernel is now represented by a compact series of exponentials, which are easy to implement in the system model.

Returning to the linear radiation force, we plug in the ESPRIT fit for the radiation kernel, and exchanging the order of summation and integration,

$$
\begin{aligned}
F_{ij,\mathrm{Rad}}(t) &= \int_{-\infty}^{t} k_{\mathrm{Rad}}(t-\tau)\,\dot{\xi}_j(\tau)\;d\tau \\
&= \int_{-\infty}^{t} \left[\sum_{n=1}^{N_{\mathrm{R}}} c_{n,\mathrm{R}} \exp\left[\beta_{n,\mathrm{R}}(t-\tau)\right]\right] \dot{\xi}_j(\tau)\;d\tau \\
&= \sum_{n=1}^{N_R} \left[\int_{-\infty}^{t} c_{n,\mathrm{R}} \exp\left[\beta_{n,\mathrm{R}}(t-\tau)\right] \dot{\xi}_j(\tau)\;d\tau\right] \\
&= \sum_{n=1}^{N_R} F_{ij,\mathrm{Rad},n}(t)\ . \qquad (4.5)
\end{aligned}
$$

Remarking on notation, the mode indices have been dropped to reduce clutter where appropriate, and the ESPRIT index n denotes the component in the last equalities of (4.5), corresponding to the convolution of the n^{th} ESPRIT exponential β_n. Note the ESPRIT coefficients will be unique to each (ij)-mode kernel.

Each $F_{ij,\mathrm{Rad},n}(t)$ represents a sub-state of the linear radiation force. Taking the derivative with respect to time,

$$
\frac{dF_{ij,\mathrm{Rad},n}(t)}{dt} = \beta_{n,\mathrm{R}} F_{ij,\mathrm{Rad},n}(t) + c_{n,\mathrm{R}} \dot{\xi}_j(t)\ . \qquad (4.6)
$$

The linear state space ODE for the force F_{Rad} follows immediately. Assemble the vector $\boldsymbol{F}_{ij,\mathrm{Rad}}(t) = [f_{\mathrm{R},1}, \ldots, f_{\mathrm{R},N_R}]^T$, the diagonal matrix $\boldsymbol{\beta}_{\mathrm{R}}$ with elements $\beta_{n,\mathrm{R}}$, and the vector $\boldsymbol{c}_{\mathrm{R}} = [c_{\mathrm{R},1}, \ldots, c_{\mathrm{R},N_R}]^T$,

$$
\frac{d}{dt}\boldsymbol{F}_{ij,\mathrm{Rad}}(t) = \boldsymbol{\beta}_{\mathrm{R}} \boldsymbol{F}_{ij,\mathrm{Rad}}(t) + \boldsymbol{c}_{\mathrm{R}} \dot{\xi}_j(t)\ . \qquad (4.7)
$$

This formulation is significant—the linear radiation force convolution has been re-

cast into a linear state space ODE, with a finite number N_{R} of states and zero mathematical memory. Now, the memory effects now are contained in the hidden states of F_{Rad}.

The causal linear excitation follows an identical derivation for its state-space realization. Skipping to the result, and using the subscript "Ex" to denote the causal excitation component,

$$\frac{d}{dt}\boldsymbol{F}_{ij,\mathrm{Ex}}(t) = \boldsymbol{\beta}_{\mathrm{Ex}}\boldsymbol{F}_{ij,\mathrm{Ex}}(t) + \boldsymbol{c}_{\mathrm{Ex}}\zeta_I(t) \ . \tag{4.8}$$

We may carry out the same procedure for the non-causal component of the linear excitation for a deterministic simulation, adding an additional term for the upper integration bound at $t + t_c$. However, we note again that in the context of the stochastic model, we need an alternative treatment of the non-causal compoments, rendering this superfluous.

4.2 Complete State-Space System

We construct the complete state-space equation of motion ODE by stacking and assembling the block-matrix state space ODEs, and the nonlinear Froude-Krylov and hydrostatic components,

$$\frac{d}{dt}\mathbb{X}(t) = \boldsymbol{A}\,\mathbb{X}(t) + \boldsymbol{B}\left(\mathbb{X}, \zeta_I(t), t\right) \ , \tag{4.9}$$

with state vector $\mathbb{X}(t)$

$$\mathbb{X}(t) = \begin{bmatrix} \boldsymbol{\xi}_i \\ \dot{\boldsymbol{\xi}}_i \\ \boldsymbol{F}_{ij,\mathrm{Rad}} \\ \boldsymbol{F}_{i,\mathrm{Ex}} \end{bmatrix}. \tag{4.10}$$

Concatenating the relevant (cross-coupled) mode ij vector and matrix components appropriately formulates the (six-degree-of-freedom) seakeeping problem for any geometry of interest, thereby achieving one of the primary goals for formulating this new framework.

The system matrix $\boldsymbol{A}$, is

$$\boldsymbol{A} = \begin{bmatrix} 0 & 1 & 0 & 0 \\ 0 & 0 & \frac{-1}{m+A_\infty}\mathbf{1} & \frac{1}{m+A_\infty}\mathbf{1} \\ 0 & \boldsymbol{c}_R & \boldsymbol{\beta}_R & 0 \\ 0 & 0 & 0 & \boldsymbol{\beta}_{Ex} \end{bmatrix} \tag{4.11}$$

The boldface $\mathbf{1}$ denotes a vector of ones with appropriate dimension. The nonlinear force vector $\boldsymbol{B}(\mathbb{X}, \zeta_I(t), t)$ is

$$\boldsymbol{B} = \begin{bmatrix} 0 \\ \frac{\boldsymbol{F}_{i,\text{F-K,nl}}(\mathbb{X},\zeta_I,t) - \boldsymbol{F}_{\mathrm{HS}}(\mathbb{X},\zeta_t)}{m+A_\infty} \\ 0 \\ \boldsymbol{c}_{\mathrm{Ex}}\zeta_I(t) + \boldsymbol{c}_{\mathrm{Ex,nc}}\zeta_I(t+t_c) \end{bmatrix} \tag{4.12}$$

The detailed treatment of the nonlinear Froude-Krylov and hydrostatic forces is left to the next section.

The hydrodynamic and state-space system model formulation is now complete. It

remains to find a stochastic model for the driving incident wave elevation $\zeta_I(t)$. The account of nonlinear inertia terms arising in Newton's law may be readily handled by the state-space formulation presented above and is omitted for clarity.

Chapter 5

The Stochastic Model

Following the new nonlinear state-space model for the deterministic seakeeping problem formulated thus far, we are now ready to introduce the last modeling step in our framework—the stochastic model. This re-formulation results in a diffusion SDE which admits solutions, either stationary or transient[1], to the FPE, that may be solved for the joint PDF of the seakeeping states. This joint PDF provides the complete space of information required to carry out a stability analysis on the vessel of interest over the set of design seastates, and thereby determine its SOE.

5.1 Ambient Seastate Model

The wave-body model presented above requires an input process for the incident wave elevation at the origin $\zeta(t)$, dropping the subindex I henceforth for simplicity. Consider a stationary, ergodic sea state, whose wave elevation is completely characterized by a spectrum $S_\zeta(\omega)$ and probability density function $p_\zeta(\zeta)$. The au-

[1]The seakeeping SDE may be non-stationary; however, we draw attention to the restriction on the input design seastate to be stationary.

tocorrelation function $R_\zeta(\tau)$, via the Wiener-Khinchin theorem, of any such real sea state is an oscillating function with a decaying envelope.

For severe seastates, assume the spectrum is narrow-banded with a maximum at the peak frequency ω_p [3]. One form of representing such a stochastic wave elevation process is

$$\zeta(t) = A(t)\cos\left[\omega_p t + \varphi(t)\right] , \tag{5.1}$$

The amplitude $A(t)$ and phase $\varphi(t)$ are stochastic processes that vary slowly in time with respect to the peak period $T_p = 2\pi/\omega_p$, and $\varphi(t) \in U[0, 2\pi)$. Primak et. al. show that a narrowband process (5.1) has an autocorrelation function of the form [19, 20],

$$R_\zeta(\tau) = \sigma_\zeta^2 e^{-\lambda|\tau|}\cos(\omega_p \tau) , \tag{5.2}$$

where $\lambda > 0$ is the exponential decay parameter. We know the left-hand-side of (5.2) in terms of the input design spectrum. Applying ESPRIT with a 2-term fit estimates the parameters ω_p and λ in (5.2), recalling that ESPRIT fits complex-conjugate pairs to a real signal.

The accuracy of the fit can be improved to within sufficiently small error by increasing the number of terms. Figure 5-1 illustrates the performance of ESPRIT using 2 and 12 terms to fit a JONSWAP spectrum with a peak frequency $\omega_p = 0.5$ rad/s and significant wave height $H_s = 8.66$ m. The 2-term fit captures the general nature of the autocorrelation, but is unable to resolve the specific peak shape. Increasing the number of terms from 2 to 12 captures the peak shape correctly, to a high degree of graphical accuracy.

To correctly perform this fit, we must make a modification to the ESPRIT algo-

rithm to force an even function to be fit, in order to be consistent with the properties of an autocorrelation function. This modification occurs in step 3 of Algorithm 3.2 derived by Potts and Tasche [17], where the Vandermonde-type system is computed using only the real part of the complex exponential.

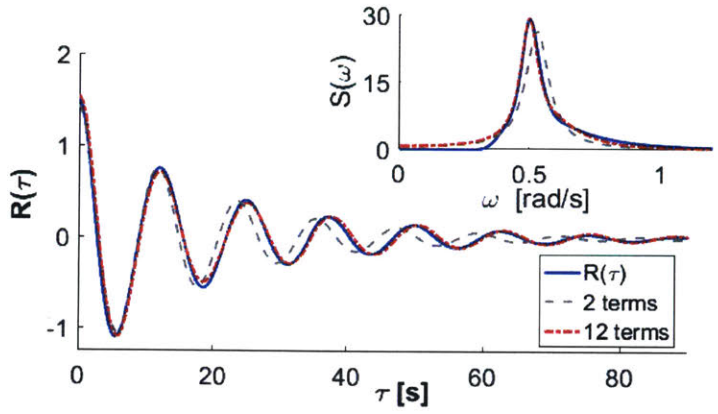

Figure 5-1: ESPRIT fit of the autocorrelation function (solid blue) corresponding to a JONSWAP spectrum with peak frequency $\omega_p = 0.5$ rad/s and significant wave height $H_s = 8.66$ m using 2 terms (dashed grey) and 12 terms (dash-dot red). The corresponding spectra (inset) illustrate that the 2-term fit captures the general spectrum shape, while the 12-term fit captures the peak shape much better.

We seek an Itô-form diffusion stochastic differential equation (SDE) to represent the ambient seastate process described by (5.1), in the form

$$d\boldsymbol{\zeta}_t = \boldsymbol{\mu}\left(\boldsymbol{\zeta}_t\right)\, dt + \boldsymbol{\sigma}\left(\boldsymbol{\zeta}_t, t\right)\, \boldsymbol{dW}_t\,. \tag{5.3}$$

The $\boldsymbol{dW}_t$ term above is a vector of independent unit white noise processes, otherwise known as unit Wiener process increments. The corresponding two-state SDE for the wave elevation process has been derived by decomposing (5.1) into components with orthogonal base-bands [21, 19, 20],

$$\begin{aligned}\zeta(t) &= A(t)\cos[\varphi(t)]\sin(\omega_p t) + A(t)\sin[\varphi(t)]\cos(\omega_p t) \\ &= \zeta_r(t) + \zeta_i(t)\ .\end{aligned} \tag{5.4}$$

ζ_r and ζ_i are shown to be solutions to the two-state diffusion-SDE [19]

$$d\begin{bmatrix}\zeta_r(t)\\ \zeta_i(t)\end{bmatrix} = \begin{bmatrix}-\lambda & \omega_p\\ -\omega_p & -\lambda\end{bmatrix}\begin{bmatrix}\zeta_r(t)\\ \zeta_i(t)\end{bmatrix}dt + \begin{bmatrix}\sigma_{11}(\boldsymbol{\zeta}(t)) & \sigma_{12}(\boldsymbol{\zeta}(t))\\ \sigma_{21}(\boldsymbol{\zeta}(t)) & \sigma_{22}(\boldsymbol{\zeta}(t))\end{bmatrix}\begin{bmatrix}dW_1(t)\\ dW_2(t)\end{bmatrix}\ . \tag{5.5}$$

By solving the associated stationary Fokker-Planck equation, Primak et. al has shown the diffusion coefficients $\boldsymbol{\sigma}$ in (5.5) to be

$$\sigma_{11}^2(\boldsymbol{\zeta}) = \frac{\lambda}{p_{\zeta_R\zeta_I}(\boldsymbol{\zeta})}\int_{-\infty}^{\zeta_R} y p_{\zeta_R\zeta_I}(y,\zeta_I)\,dy \tag{5.6a}$$

$$\sigma_{22}^2(\boldsymbol{\zeta}) = \frac{\lambda}{p_{\zeta_R\zeta_I}(\boldsymbol{\zeta})}\int_{-\infty}^{\zeta_I} y p_{\zeta_R\zeta_I}(\zeta_R,y)\,dy \tag{5.6b}$$

$$\sigma_{12}^2(\boldsymbol{\zeta}) = \sigma_{21}^2(\boldsymbol{\zeta}) = \frac{\omega_p}{p_{\zeta_R\zeta_I}(\boldsymbol{\zeta})}\left[\int_{-\infty}^{\zeta_I} y p_{\zeta_R\zeta_I}(\zeta_R,y)\,dy - \int_{-\infty}^{\zeta_R} y p_{\zeta_R\zeta_I}(y,\zeta_I)\,dy\right]\ . \tag{5.6c}$$

The joint PDF $p_{\zeta_R\zeta_I}(\boldsymbol{\zeta})$ in (5.6) was derived from $p_\zeta(\zeta)$ by Primak et. al. as follows [20]. Given $\varphi(t)$ is uniformly distributed over $[0, 2\pi)$, the PDF of the envelope $A(t)$ is found by applying the Blanc-Lapierre Transform,

$$p_A(A) = A\int_{-\infty}^{\infty}\int_{-\infty}^{\infty}\eta p_\zeta(y) J_0(\eta A) e^{i\eta y}\,d\eta\,dy\ . \tag{5.7}$$

$A(t)$ and $\varphi(t)$ are assumed independent,

$$p_{A,\varphi}(A,\varphi) = \frac{1}{2\pi} p_A(A) \ , \tag{5.8}$$

and by a Jacobian transformation using (5.4), he arrives at,

$$p_{\zeta_R\zeta_I}(\zeta_R,\zeta_I) = \frac{1}{2\pi} \frac{p_A\left(\sqrt{\zeta_R^2+\zeta_I^2}\right)}{\sqrt{\zeta_R^2+\zeta_I^2}} \ . \tag{5.9}$$

Note the process generated by the SDE (5.5) may admit a wide range of distributions, where the diffusion coefficients, in general, are computed numerically.

In the special, but widely useful, case when ζ_t is Gaussian-distributed, the diffusion terms have analytic solutions, and are in fact constant,

$$\sigma_{11} = \sigma_{22} = \sigma_\zeta \sqrt{2\lambda} \tag{5.10a}$$
$$\sigma_{12} = \sigma_{21} = 0 \ . \tag{5.10b}$$

We note σ_ζ^2 is the variance of the Gaussian seastate process ζ_t, drawing the distinction from the diffusion coefficients $\boldsymbol{\sigma}(\boldsymbol{\zeta})$. Figure 6-1 in Section 6 shows a numerical simulation of (5.5) with a peak frequency of $\omega_p = 0.5$ [rad/s] and decay $\lambda = 0.05$, corresponding to a significant wave height of $H_s = 8.9$ [m].

We now assume the seastate is Gaussian for the remainder of this work.

Under the condition of a Gaussian seastate, we may relax the narrow-banded assumption as needed. Consider a seastate autocorrelation function requiring $N > 2$ ESPRIT terms for an accurate representation. Each pair comprises an independent frequency component of the autocorrelation function. Given that the Gaussian distribution is a stable distribution, i.e. the sum of independent Gaussian random variables is again Gaussian; the complete wide-band process can be constructed as the sum of $k = N/2$ independent component processes,

$$\zeta(t) = \zeta_1(t) + \zeta_2(t) + ... + \zeta_k(t) \ . \tag{5.11}$$

This is in essence, an extension of the classical St Denis and Pierson model [4] for a stochastic seastate, generalized under a Gaussian narrow-band SDE, instead of sinusoids with uniform random phases. The corresponding N-dimensional vector SDE has block-matrix drift and diffusion terms

$$d\begin{bmatrix}\zeta_1(t)\\ \zeta_2(t)\\ \vdots\\ \zeta_k(t)\end{bmatrix} = \begin{bmatrix}\mu_1(\zeta_1(t)) & 0 & \dots & 0\\ 0 & \mu_2(\zeta_2(t)) & \dots & 0\\ \vdots & \vdots & \ddots & \vdots\\ 0 & 0 & \dots & \mu_k(\zeta_k(t))\end{bmatrix}\begin{bmatrix}\zeta_1(t)\\ \zeta_2(t)\\ \vdots\\ \zeta_k(t)\end{bmatrix} dt + \begin{bmatrix}\sigma_1(\zeta_1(t)) & 0 & \cdots & 0\\ 0 & \sigma_2(\zeta_2(t)) & \cdots & 0\\ \vdots & \vdots & \ddots & \vdots\\ 0 & 0 & \cdots & \sigma_k(\zeta_k(t))\end{bmatrix} \boldsymbol{dW}_t \,. \tag{5.12}$$

Note that while block-seastate processes may be formulated, it is desirable to use a minimum number of states for computational efficiency and compactness, and therefore we assume a two-state seastate model henceforth for illustrative purposes.

5.1.1 Conversion to Stratonovich-Form

The process presented by Primak et. al. in (5.5), defined using the Itô-form of the stochastic integral, may be transformed into the Stratonovich form,

$$d\boldsymbol{\zeta}_t = \hat{\boldsymbol{\mu}}\left(\boldsymbol{\zeta}_t\right)\, dt + \boldsymbol{\sigma}\left(\boldsymbol{\zeta}_t\right) \circ \boldsymbol{dW}_t \tag{5.13}$$

using the corrected drift coefficients [10],

$$\hat{\mu}_i(\boldsymbol{\zeta}_t) = \mu_i(\boldsymbol{\zeta}_t) - \frac{1}{2}\sum_{j=1}^{2}\sum_{k=1}^{2}\sigma_{jk}(\boldsymbol{\zeta}_t)\frac{\partial\sigma_{ik}(\boldsymbol{\zeta}_t)}{\partial\zeta_j} . \tag{5.14}$$

The seastate in Stratonovich form is then,

$$d\begin{bmatrix}\zeta_R(t)\\ \zeta_I(t)\end{bmatrix} = \begin{bmatrix}-\lambda & \omega_p\\ -\omega_p & -\lambda\end{bmatrix}\begin{bmatrix}\zeta_r(t)\\ \zeta_i(t)\end{bmatrix}dt + \begin{bmatrix}\sigma_\zeta\sqrt{2\lambda} & 0\\ 0 & \sigma_\zeta\sqrt{2\lambda}\end{bmatrix}\circ\begin{bmatrix}dW_1(t)\\ dW_2(t)\end{bmatrix} . \tag{5.15}$$

The $\circ$ symbol denotes a Stratonovich integral. Note that a Gaussian process has the same drift coefficients in both the the Itô and Stratonovich forms, as the diffusion terms are constant.

5.2 Building a Stochastic Differential Equation for the State-Space System

Combining the state-space system (4.9) with the seastate model forms a multi-dimensional SDE in the general Stratonovich form with a modified state-vector $\mathbb{X}_t$,

$$d\mathbb{X}_t = \boldsymbol{\mu}(\mathbb{X}_t, t)\ dt + \boldsymbol{\sigma}(\mathbb{X}_t, t)\circ d\boldsymbol{W}_t . \tag{5.16}$$

In order for the process $\mathbb{X}_t$ to satisfy (5.16), it must be an adapted process. Additionally, to satisfy the Fokker-Planck equation[2] in a tractable form, it must be a (semi-)martingale, satisfying the Markov property. We have already taken care of

[2]There exist generalized Fokker-Planck equations for processes with memory, however they have limited extensions to multidimensional systems.

this second requirement with respect to the linear system by converting the linear convolutions to state space form, however we must still address several aspects of the linear and nonlinear state-space model presented in (4.9) to satisfy both requirements (please refer to Øksendal, 2010 and Stratonovich, 1966 for further detail) [8, 9].

5.2.1 Treatment of Linear Excitation Non-Causality

First, the multidimensional state-vector process $\mathbb{X}_t$ must be an adapted process. An adapted process is a non-anticipatory (or causal) process. Therefore, we resolve the non-causality in the convolution integrals presented above with the following treatment.

As the seastate ζ_t considered here is Gaussian, $\zeta(t) = \zeta_t$ and $\zeta(t+\vartheta) = \zeta_{t+\vartheta}$ are jointly Gaussian processes. It follows that the joint PDF is

$$p_{\zeta_t \zeta_{t+\vartheta}}(\zeta_t, \zeta_{t+\vartheta}) = \frac{1}{2\pi\sigma_\zeta^2\sqrt{1-\rho_\zeta(\vartheta)^2}} \exp\left[-\frac{\zeta_t^2 + \zeta_{t+\vartheta}^2 - 2\rho_\zeta(\vartheta)\,\zeta_t\zeta_{t+\vartheta}}{2\sigma_\zeta^2\left(1-\rho_\zeta(\vartheta)^2\right)}\right], \quad (5.17)$$

where correlation coefficient $\rho_\zeta(\vartheta)$ is known,

$$\rho_\zeta(\vartheta) = \frac{R_\zeta(\vartheta)}{\sigma_\zeta^2}. \quad (5.18)$$

Recall the non-causal excitations (3.5) have already been decomposed into a causal term and a non-causal term. We now replace the future wave elevation $\zeta_I(\tau)\ \ \tau > t$ in the non-causal integral with its expectation, conditional on the wave elevation at time t,

$$E\left[\zeta(t+\vartheta)\,|\zeta(t)\right] = \rho_\zeta(\vartheta)\zeta_t. \quad (5.19)$$

Substituting (5.19) into (3.5),

$$
\begin{aligned}
F_{i,\text{Ex,non-causal}}(t) &= \int_{t}^{t+t_c} k_{i,\text{Ex}}(t-\tau)\,\zeta(\tau)\;d\tau \\
&= \int_{t}^{t+t_c} k_{i,\text{Ex}}(t-\tau)\,\rho_{\zeta}(t-\tau)\,\zeta_t\;d\tau \\
&= \zeta_t \int_{0}^{t_c} k_{i,\text{Ex}}(u)\,\rho_{\zeta}(u)\;du = \zeta_t \mathbb{C}_{i,\text{Ex}}
\end{aligned}
\tag{5.20}
$$

This reduces the non-causality to a causal approximation, which for the linear excitation remains linear in ζ_t. Furthermore, this approximation justifies the earlier decision to perform an ESPRIT fit for only the causal component of the linear non-causal kernels. As we may pre-compute the coefficients $\mathbb{C}_{i,\text{Ex}}$ in (5.20), we use the exact non-causal part of the kernels directly.

5.2.2 Nonlinear Froude-Krylov and Hydrostatics

To ensure the Markov property is satisfied, we introduce an alternative representation for the nonlinear Froude-Kylov and hydrostatic components hinted at in Section 3.2. Recall the nonlinear Froude-Krylov and hydrostatic roll moments may be represented in the form

$$
F_{4,\text{F-K,nl}}(t) = -\rho \int_{\bar{S}_w} \left[\left(\frac{\partial \zeta_I(y,t)}{\partial t} \right)^2 + \frac{\partial^2 \zeta_I(y,t)}{\partial t^2} \zeta_I(y,t) \right] y\,ds\,. \tag{5.21}
$$

and

$$
F_{4,HS}(t) = \rho g \int_{\bar{S}_w} \zeta_I(y,t)\,y\,dy \tag{5.22}
$$

respectively. To treat these in the stochastic sense, we consider a discrete mesh of the interval $\bar{S}_w$ in (3.21) from $m = 1, \ldots, M$, and introduce the following functions as additional state variables,

$$\kappa_{0,m}(t) \equiv \zeta_I(y_m, t) \tag{5.23a}$$

$$\kappa_{1,m}(t) \equiv \frac{\partial \zeta_I(y_m, t)}{\partial t} \tag{5.23b}$$

$$\kappa_{2,m}(t) \equiv \frac{\partial^2 \zeta_I(y_m, t)}{\partial t^2}\,, \tag{5.23c}$$

The nonlinear Froude-Krylov follows immediately in the form

$$F_{4,\text{F-K,nl}}(t) = \rho \sum_{m=1}^{M} \left[\kappa_{1,m}^2(t) + \kappa_{0,m}(t)\,\kappa_{2,m}(t)\right] y_m\,\Delta y_m\,. \tag{5.24}$$

and the nonlinear hydrostatics,

$$F_{4,HS}(t) = \rho g \sum_{m=1}^{M} \kappa_{0,m}(t)\, y_m \Delta y_m\,. \tag{5.25}$$

The states $\kappa_0(t)$, $\kappa_1(t)$ and $\kappa_2(t)$ are stochastic processes, modeled with the same formulation as the incident wave elevation ζ_t, and correlated with the wave elevation at the origin, ζ_t. To avoid confusion by carrying too many indices, the processes defined in (5.23) will be referred to as the "κ-auxiliary-processes," with the generalized index q denoting any of $\kappa_{0,m}$, $\kappa_{1,m}$ and $\kappa_{2,m}$ for the remainder of this derivation.

Looking into the correlation structure of the auxiliary processes further, by virtue of linearity, we can compute the autocorrelation functions and cross-correlation functions of these new states with ζ_t by applying the Wiener-Khinchin theorem [22],

$$R_{\zeta q}(\tau) = \Re\left\{\frac{1}{2\pi}\int_{-\infty}^{\infty} S_{\zeta q}(\omega)\, e^{i\omega\tau}\, d\omega\right\} \tag{5.26}$$

To compute (5.26), we easily see from linear theory that transfer functions $H_{\zeta q}$ between each auxiliary process κ_q and the "anchor" wave elevation process ζ are,

$$H_{\zeta 0_m}(\omega) = e^{-ik_p y_m} \tag{5.27a}$$
$$H_{\zeta 1_m}(\omega) = i\omega e^{-ik_p y_m} \tag{5.27b}$$
$$H_{\zeta 2_m}(\omega) = -\omega^2 e^{-ik_p y_m} \tag{5.27c}$$

Therefore, the cross-spectra are,

$$S_{\zeta q} = H_{\zeta q}(\omega) S_\zeta(\omega) \tag{5.28}$$

And by applying the time-derivative property of the Fourier transform, the cross-correlations are

$$\begin{aligned} R_{\zeta 0_m}(\tau) &= \cos(k_p y_m) R_\zeta(\tau) \\ &= \sigma_\zeta^2 \exp(-\lambda|\tau|) \cos(\omega_p \tau) \end{aligned} \tag{5.29a}$$

$$\begin{aligned} R_{\zeta 1_m}(\tau) &= \cos(k_p y_m) \frac{dR_\zeta(\tau)}{d\tau} \\ &= -\sigma_\zeta^2 \cos(k_p y_m) \exp(-\lambda\tau) \left[\lambda \cos(\omega_p \tau) + \omega_p \sin(\omega_p \tau)\right], \ \tau \geq 0 \end{aligned} \tag{5.29b}$$

$$\begin{aligned} R_{\zeta 2_m}(\tau) &= \cos(k_p y_m) \frac{d^2 R_\zeta(\tau)}{d\tau^2} \\ &= \sigma_\zeta^2 \cos(k_p y_m) \exp(-\lambda\tau) \left[\left(\lambda^2 - \omega_p^2\right) \cos(\omega_p \tau) + 2\lambda\omega_p \sin(\omega_p \tau)\right], \ \tau \geq 0 \end{aligned} \tag{5.29c}$$

Similarly, the spectrum of each auxiliary process is

$$S_{\kappa_q}(\omega) = H_{\zeta q} H_{\zeta q}^* S_\zeta(\omega) \tag{5.30}$$

The variance is simply the integral of the spectrum,

$$\sigma_{\kappa_q}^2 = \int_0^\infty S_{\kappa_q}(\omega) \, d\omega \tag{5.31}$$

Putting the pieces together, we use the variance of the anchor wave elevation σ_ζ^2 and of the auxiliary processes $\sigma_{\kappa_j}^2$ to realize the normalized correlation coefficients,

$$\rho_{\zeta q} = \frac{R_{\zeta q}(0)}{\sigma_\zeta \sigma_{\kappa_q}} \tag{5.32}$$

The correlation coefficients between the auxiliary-states may also be computed in an analogous way, resulting in complete knowledge of the correlation matrix $\boldsymbol{C}$ between the wave elevation process ζ and κ-auxiliary-processes. Although, this will not be necessary in our construction that follows. Additionally, we also know the correlation structure as a function of the lag variable τ. However, the question remains, what does an SDE for such a wave elevation and auxiliary process system look like?

5.2.3 Derivation of the Correlated Seastate Sub-Process System

It is thus necessary for us to represent the extended seastate-plus-κ-auxiliary-process model as a linear Itô SDE

$$d\mathbb{Y}_t = \boldsymbol{L}\mathbb{Y}_t dt + \boldsymbol{G}\, \boldsymbol{dW}_t \tag{5.33}$$

which is then straightforward to convert to the Stratonovich form before inserting it into the complete system SDE. The matrix $\boldsymbol{L}$ is a linear drift, and $\boldsymbol{G}$ is a constant diffusion matrix. The time-dependent mean $\boldsymbol{M}$ and covariance $\mathbb{K}$ matrices of the process $\mathbb{Y}_t$ satisfying (5.38) also satisfy the differential equations [23],

$$\frac{d\boldsymbol{M}_t}{dt} = \boldsymbol{L}\boldsymbol{M}_t \tag{5.34a}$$

$$\frac{d\mathbb{K}_t}{dt} = \boldsymbol{L}\mathbb{K}_t + \mathbb{K}_t\boldsymbol{L}^T + \boldsymbol{G}\boldsymbol{G}^T \tag{5.34b}$$

As the κ-auxiliary-processes are stationary by nature of the wave elevation being stationary, the mean and autocorrelation functions are time-independent, which requires the left hand side of (5.34a) and (5.34b) to be zero. This results in zero mean processes as expected, and a Lyapunov-type equation for the covariance matrix,

$$\boldsymbol{L}\mathbb{K}_t + \mathbb{K}_t\boldsymbol{L}^T + \boldsymbol{G}\boldsymbol{G}^T = 0 \tag{5.35}$$

The SDE (5.38) is not uniquely determined by (5.35) and (5.34a). To proceed, we assume the two-dimensional SDE (5.5) to be the building block to construct the drift $\boldsymbol{L}$ and diffusion $\boldsymbol{G}$ terms.

Each κ-auxiliary-process is represented by a narrowband process of the form

$$\kappa_q(t) = A_q(t)\cos\left[\omega_p t - k_p y_q + \varphi_q + \varphi(t)\right] \tag{5.36}$$

where $A_q(t) \equiv c_q A(t)$ is the slowly-varying amplitude process. The coefficient c_q absorbs the gain of the transfer function $H_{\zeta q}$ and the phase φ_q is induced by $H_{\zeta q}$. Analogous to the wave elevation, we decompose κ_q into orthogonal base-band components,

$$\begin{aligned}\kappa_q(t) &= A_q(t)\cos\left[\varphi(t)\right]\sin\left(\omega_p t - k_p y_q + \varphi_q\right) + A_q(t)\sin\left[\varphi(t)\right]\cos\left(\omega_p t - k_p y_q + \varphi_q\right) \\ &= \kappa_q^{(R)} + \kappa_q^{(I)}\end{aligned} \tag{5.37}$$

Without loss of generality, temporarily consider the constant phase $-k_p y_q + \varphi_q$ is absorbed into the stochastic phase $\varphi(t)$. The process $\kappa_q(t)$ now looks identical to the wave elevation process $\zeta(t)$, and therefore can be individually represented by the

two-dimensional SDE

$$d\begin{bmatrix}\kappa_q^{(R)}\\ \kappa_q^{(I)}\end{bmatrix} = \begin{bmatrix}-\lambda_q & \omega_p\\ -\omega_p & -\lambda_q\end{bmatrix}\begin{bmatrix}\kappa_q^{(R)}\\ \kappa_q^{(I)}\end{bmatrix}dt + \begin{bmatrix}\sigma_q\sqrt{2\lambda_q} & 0\\ 0 & \sigma_q\sqrt{2\lambda_q}\end{bmatrix}\begin{bmatrix}dV_{1,t}\\ dV_{2,t}\end{bmatrix} \tag{5.38}$$

where $dV_{1,t}$ and $dV_{2,t}$ are unit white noise processes independent from each other. The process $\kappa_q = \kappa_q^{(R)} + \kappa_q^{(I)}$ described by (5.38) admits the correct autocorrelation function described by the inverse Fourier transform of (5.30). We draw attention to the subtle difference between (5.38) and (5.5), in the use of the vector $\boldsymbol{dV}_t^{(q)}$ instead of $\boldsymbol{dW}_t$. We purposefully reserve the vector $\boldsymbol{dW}_t$ to denote a vector of independent unit white noise processes. We now choose to introduce the pair-wise correlation of the *q-th* κ-auxiliary-process with the anchoring wave elevation process ζ_t by pair-wise correlating the white noise processes $\boldsymbol{dV}_t^{(q)}$ with the white noise processes $\boldsymbol{dW}_t^{(\zeta)}$ belonging to ζ_t. It suffices to pair-wise correlate auxiliary processes to the anchor process using the following orthogonal decomposition, through which process, all auxiliary processes will be appropriately correlated to each other.

In the most general form, we assume $\boldsymbol{dV}_t^{(q)}$ is represented by

$$\begin{bmatrix}dV_1^{(q)}\\ dV_2^{(q)}\end{bmatrix} = \begin{bmatrix}\rho_{\zeta_1 q_1} & \rho_{\zeta_2 q_1} & \left(1-\rho_{\zeta_1 q_1}^2-\rho_{\zeta_2 q_1}^2\right)^{\frac{1}{2}} & 0\\ \rho_{\zeta_1 q_2} & \rho_{\zeta_2 q_2} & 0 & \left(1-\rho_{\zeta_1 q_2}^2-\rho_{\zeta_2 q_2}^2\right)^{\frac{1}{2}}\end{bmatrix}\begin{bmatrix}dW_1^{(\zeta)}\\ dW_2^{(\zeta)}\\ dW_1^{(q)}\\ dW_2^{(q)}\end{bmatrix} \tag{5.39}$$

recalling that the components $\boldsymbol{dW}_t = \left[dW_1^{(\zeta)}\ dW_2^{(\zeta)}\ dW_1^{(q)}\ dW_2^{(q)}\right]^T$ are independent. From inspection, for the components of $\boldsymbol{dV}_t^{(q)}$ to be independent (and by inverse

arguments, for the components of $\boldsymbol{dW}_t$ to be independent), neither element of the same row of the 2-by-2 sub-matrix

$$\hat{\boldsymbol{\rho}}_{\boldsymbol{\zeta q}} = \begin{bmatrix} \rho_{\zeta_1 q_1} & \rho_{\zeta_2 q_1} \\ \rho_{\zeta_1 q_2} & \rho_{\zeta_2 q_2} \end{bmatrix} \tag{5.40}$$

may be simultaneously non-zero. In the trivial case that the cross-correlation coefficient $\rho_{\zeta q} = 0$, all of the components of $\hat{\boldsymbol{\rho}}_{\boldsymbol{\zeta q}}$ are identically zero. When $\rho_{\zeta q}$ is finite, we find the relationship between the sub-state correlations and auxiliary-process correlations by taking the expectation. Opening up the parentheses and using the linear property of the expectation operator,

$$\begin{aligned} \rho_{\zeta q} &= E\left[\left(dW_1 + dW_2\right)\left(dV_1 + dV_2\right)\right] \\ &= E\left[dW_1\, dV_1\right] + E\left[dW_1\, dV_2\right] + E\left[dW_2\, dV_1\right] + E\left[dW_2\, dV_2\right] \\ &= \rho_{\zeta_1 q_1} + \rho_{\zeta_2 q_1} + \rho_{\zeta_1 q_2} + \rho_{\zeta_2 q_2} \\ &= \begin{cases} \rho_{\zeta_1 q_1} + \rho_{\zeta_2 q_2}, & \rho_{\zeta_2 q_1} = \rho_{\zeta_1 q_2} = 0 \\ \rho_{\zeta_2 q_1} + \rho_{\zeta_1 q_2}, & \rho_{\zeta_1 q_1} = \rho_{\zeta_2 q_2} = 0 \end{cases} \end{aligned} \tag{5.41}$$

Simultaneously, we can compute the right-hand-side of (5.41) by directly calculating the time-series cross-correlation coefficients between the components of (5.4) and (5.37),

$$\rho_{\zeta_1 q_1} = \frac{c_q}{\sigma_\zeta \sigma_{\kappa_q}} \int_{-\infty}^{\infty} A^2(t) \cos^2\left[\varphi(t)\right] \sin\left(\omega_p t\right) \sin\left(\omega_p t - k_p y_q + \varphi_q\right)\, dt \tag{5.42a}$$

$$\rho_{\zeta_2 q_2} = \frac{c_q}{\sigma_\zeta \sigma_{\kappa_q}} \int_{-\infty}^{\infty} A^2(t) \sin^2\left[\varphi(t)\right] \cos\left(\omega_p t\right) \cos\left(\omega_p t - k_p y_q + \varphi_q\right)\, dt \tag{5.42b}$$

$$\rho_{\zeta_2 q_1} = \frac{c_q}{\sigma_\zeta \sigma_{\kappa_q}} \int_{-\infty}^{\infty} A^2(t) \cos[\varphi(t)] \sin[\varphi(t)] \cos(\omega_p t) \sin(\omega_p t - k_p y_q + \varphi_q)\, dt \quad (5.42c)$$

$$\rho_{\zeta_1 q_2} = \frac{c_q}{\sigma_\zeta \sigma_{\kappa_q}} \int_{-\infty}^{\infty} A^2(t) \sin[\varphi(t)] \cos[\varphi(t)] \sin(\omega_p t) \cos(\omega_p t - k_p y_q + \varphi_q)\, dt \quad (5.42d)$$

Applying the difference angle trigonometric relations,

$$\rho_{\zeta_1 q_1} = \frac{c_q}{\sigma_\zeta \sigma_{\kappa_q}} \int_{-\infty}^{\infty} A^2(t) \cos^2[\varphi(t)] \sin(\omega_p t) [\sin(\omega_p t) \cos(k_p y_q - \varphi_q) - \cos(\omega_p t) \sin(k_p y_q - \varphi_q)]\, dt \quad (5.43a)$$

$$\rho_{\zeta_2 q_2} = \frac{c_q}{\sigma_\zeta \sigma_{\kappa_q}} \int_{-\infty}^{\infty} A^2(t) \sin^2[\varphi(t)] \cos(\omega_p t) [\cos(\omega_p t) \cos(k_p y_q - \varphi_q) + \sin(\omega_p t) \sin(k_p y_q - \varphi_q)]\, dt \quad (5.43b)$$

$$\rho_{\zeta_2 q_1} = \frac{c_q}{\sigma_\zeta \sigma_{\kappa_q}} \int_{-\infty}^{\infty} A^2(t) \cos[\varphi(t)] \sin[\varphi(t)] \cos(\omega_p t) [\sin(\omega_p t) \cos(k_p y_q - \varphi_q) - \cos(\omega_p t) \sin(k_p y_q - \varphi_q)]\, dt \quad (5.43c)$$

$$\rho_{\zeta_1 q_2} = \frac{c_q}{\sigma_\zeta \sigma_{\kappa_q}} \int_{-\infty}^{\infty} A^2(t) \sin[\varphi(t)] \cos[\varphi(t)] \sin(\omega_p t) [\cos(\omega_p t) \cos(k_p y_q - \varphi_q) + \sin(\omega_p t) \sin(k_p y_q - \varphi_q)]\, dt \quad (5.43d)$$

Dropping orthogonal terms leaves

$$\rho_{\zeta_1 q_1} = \frac{c_q \cos\left(k_p y_q - \varphi_q\right)}{\sigma_\zeta \sigma_{\kappa_q}} \int_{-\infty}^{\infty} A^2\left(t\right) \cos^2\left[\varphi\left(t\right)\right] \sin^2\left(\omega_p t\right)\, dt \tag{5.44a}$$

$$\rho_{\zeta_2 q_2} = \frac{c_q \cos\left(k_p y_q - \varphi_q\right)}{\sigma_\zeta \sigma_{\kappa_q}} \int_{-\infty}^{\infty} A^2\left(t\right) \sin^2\left[\varphi\left(t\right)\right] \cos^2\left(\omega_p t\right)\, dt \tag{5.44b}$$

$$\rho_{\zeta_2 q_1} = \frac{c_q \sin\left(k_p y_q - \varphi_q\right)}{\sigma_\zeta \sigma_{\kappa_q}} \int_{-\infty}^{\infty} A^2\left(t\right) \cos\left[\varphi\left(t\right)\right] \sin\left[\varphi\left(t\right)\right] \cos^2\left(\omega_p t\right)\, dt \tag{5.44c}$$

$$\rho_{\zeta_1 q_2} = \frac{c_q \sin\left(k_p y_q - \varphi_q\right)}{\sigma_\zeta \sigma_{\kappa_q}} \int_{-\infty}^{\infty} A^2\left(t\right) \sin\left[\varphi\left(t\right)\right] \cos\left[\varphi\left(t\right)\right] \sin^2\left(\omega_p t\right)\, dt \tag{5.44d}$$

Finally, the remaining integrals are the base-band covariances, or equivalently, half the wave elevation variance. We clearly recognize $\sigma_{\kappa_q} = c_q \sigma_\zeta$, leaving the final result,

$$\rho_{\zeta_1 q_1} = \frac{1}{2} \cos\left(k_p y_q - \varphi_q\right) \tag{5.45a}$$

$$\rho_{\zeta_2 q_2} = \frac{1}{2} \cos\left(k_p y_q - \varphi_q\right) \tag{5.45b}$$

$$\rho_{\zeta_2 q_1} = \rho_{\zeta_1 q_2} = 0 \tag{5.45c}$$

Carrying out the above procedure for all $q = 1, 2, \ldots, Q$, we stack the resulting

pair-wise coupled processes, forming the white-noise correlation system,

$$\begin{bmatrix} dW_1 \\ dW_2 \\ dV_1^{(1)} \\ dV_2^{(1)} \\ \vdots \\ dV_1^{(Q)} \\ dV_2^{(Q)} \end{bmatrix} = \bar{\boldsymbol{\rho}}_{\zeta\kappa_q} \begin{bmatrix} dW_1 \\ dW_2 \\ dW_1^{(1)} \\ dW_2^{(1)} \\ \vdots \\ dW_1^{(Q)} \\ dW_2^{(Q)} \end{bmatrix} \tag{5.46a}$$

$$\bar{\boldsymbol{\rho}}_{\zeta\kappa_q} = \begin{bmatrix} 1 & 0 & 0 & 0 & \cdots & 0 & 0 \\ 0 & 1 & 0 & 0 & \cdots & 0 & 0 \\ \rho_{\zeta_1 1_1} & 0 & \left(1-\rho_{\zeta_1 1_1}^2\right)^{\frac{1}{2}} & 0 & \cdots & 0 & 0 \\ 0 & \rho_{\zeta_2 1_2} & 0 & \left(1-\rho_{\zeta_2 1_2}^2\right)^{\frac{1}{2}} & \cdots & 0 & 0 \\ \vdots & \vdots & \vdots & \vdots & \ddots & \vdots & \vdots \\ \rho_{\zeta_1 Q_1} & 0 & 0 & 0 & \cdots & \left(1-\rho_{\zeta_1 Q_1}^2\right)^{\frac{1}{2}} & 0 \\ 0 & \rho_{\zeta_1 Q_2} & 0 & 0 & \cdots & 0 & \left(1-\rho_{\zeta_2 Q_2}^2\right)^{\frac{1}{2}} \end{bmatrix} \tag{5.46b}$$

The modified form of (5.38) for the wave elevation process and auxiliary κ-auxiliary-processes follows,

$$d\mathbb{Y}_t = \boldsymbol{L}\mathbb{Y}_t dt + \left(\boldsymbol{G}\,\bar{\boldsymbol{\rho}}_{\boldsymbol{\zeta\kappa_q}}\right)\,\boldsymbol{dW}_t \tag{5.47}$$

$\boldsymbol{L}$ and $\boldsymbol{G}$ are block matrices comprised of the 2D narrowband SDEs,

$$\boldsymbol{L} = \begin{bmatrix} -\lambda & \omega_p & 0 & 0 & \cdots & 0 & 0 \\ -\omega_p & -\lambda & 0 & 0 & \cdots & 0 & 0 \\ 0 & 0 & -\lambda_1 & \omega_p & \cdots & 0 & 0 \\ 0 & 0 & -\omega_p & -\lambda_1 & \cdots & 0 & 0 \\ \vdots & \vdots & \vdots & \vdots & \ddots & \vdots & \vdots \\ 0 & 0 & 0 & 0 & \cdots & -\lambda_Q & \omega_p \\ 0 & 0 & 0 & 0 & \cdots & -\omega_p & -\lambda_Q \end{bmatrix} \tag{5.48a}$$

$$\boldsymbol{G} = \begin{bmatrix} \sigma_\zeta\sqrt{2\lambda} & 0 & 0 & 0 & \cdots & 0 & 0 \\ 0 & \sigma_\zeta\sqrt{2\lambda} & 0 & 0 & \cdots & 0 & 0 \\ 0 & 0 & \sigma_1\sqrt{2\lambda_1} & 0 & \cdots & 0 & 0 \\ 0 & 0 & 0 & \sigma_1\sqrt{2\lambda_1} & \cdots & 0 & 0 \\ \vdots & \vdots & \vdots & \vdots & \ddots & \vdots & \vdots \\ 0 & 0 & 0 & 0 & \cdots & \sigma_Q\sqrt{2\lambda_Q} & 0 \\ 0 & 0 & 0 & 0 & \cdots & 0 & \sigma_Q\sqrt{2\lambda_Q} \end{bmatrix} \tag{5.48b}$$

Remarking on the structure of these matrices, the upper left 2-by-2 matrix in $\boldsymbol{L}$ and $\boldsymbol{G}\,\bar{\boldsymbol{\rho}}_{\boldsymbol{\zeta\kappa_q}}$ is simply $\boldsymbol{\mu}_\zeta$, and $\boldsymbol{\sigma}_\zeta$, respectively.

We add a few concluding comments on the physical nature of this system. We cannot say anything further than the processes represented by (5.47) converge in distribution to the deterministic discretized Froude-Krylov auxiliary states over the mesh m. However, when the correlation between the y_m spatial nodes of the same order derivative of $\zeta(y,t)$ is nearly 1, the majority of the stochastic evolution weight is placed on $\boldsymbol{dW}_t^{(\zeta)}$. Therefore, we expect something closer to almost sure conver-

gence of the trajectories of the κ-auxiliary-processes to the paths of the deterministic discrete Froude-Krylov states, with respect to a driving wave elevation measured at the origin.

The derivation of the correlated κ-auxiliary-process SDE is now complete, and with that, all the components of our SDE system have now been found.

5.2.4 The Complete System SDE

We now form a multidimensional SDE for the state-space system by concatenating the deterministic state-space model (4.9) and the ambient incident seastate SDE, written in standard array-notation,

$$d\mathbb{X}_t = \boldsymbol{\mu}\left(\mathbb{X}_t, t\right)\, dt + \boldsymbol{\sigma}\left(\mathbb{X}_t\right) \circ \boldsymbol{dW}_t \,. \tag{5.49}$$

The $\boldsymbol{dW}_t$ term is a vector of independent unit white-noise processes of equal dimension to the number of states in $\mathbb{X}$. The process $\mathbb{X}_t$ has states

$$\mathbb{X}_t = \begin{bmatrix} \boldsymbol{\xi}_i & \dot{\boldsymbol{\xi}}_i & \boldsymbol{F}_{ij,\mathrm{Rad}} & \boldsymbol{F}_{i,\mathrm{Ex}} & \boldsymbol{\zeta}_t & \boldsymbol{\kappa}_{0,t} & \boldsymbol{\kappa}_{1,t} & \boldsymbol{\kappa}_{2,t} \end{bmatrix}^T \,, \tag{5.50}$$

where $\boldsymbol{\zeta}_t$ and $\kappa_{q,t}$ are now also states. Note the matrices in the previous subsection should be appropriately arranged to this form. The drift array looks similar to the deterministic state-space system matrix, with the inclusion of the incident wave elevation substates and κ-auxiliary-process substates as stochastic state variables,

$$\boldsymbol{\mu}\left(\mathbb{X}_t\right) = \hat{\boldsymbol{\mu}}\, \mathbb{X}_t + \bar{\boldsymbol{\mu}}\left(\mathbb{X}_t\right) \tag{5.51a}$$

$$\hat{\boldsymbol{\mu}} = \begin{bmatrix} 0 & 1 & 0 & 0 & 0 & 0 & 0 & 0 \\ 0 & 0 & \frac{-1}{m+A_\infty}\mathbf{1} & \frac{1}{m+A_\infty}\mathbf{1} & 0 & \frac{-\rho g}{m+A_\infty}\boldsymbol{y}_m & 0 & 0 \\ 0 & \boldsymbol{c}_R & \boldsymbol{\beta}_R & 0 & 0 & 0 & 0 & 0 \\ 0 & 0 & 0 & \boldsymbol{\beta}_{Ex} & \boldsymbol{c}_{\mathrm{Ex}} + \boldsymbol{C}_{\mathrm{Ex}} & 0 & 0 & 0 \\ 0 & 0 & 0 & 0 & \boldsymbol{\mu}_\zeta & 0 & 0 & 0 \\ 0 & 0 & 0 & 0 & 0 & \multicolumn{3}{c}{\multirow{3}{*}{$\overline{\boldsymbol{L}}$}} \\ 0 & 0 & 0 & 0 & 0 & & & \\ 0 & 0 & 0 & 0 & 0 & & & \end{bmatrix}. \tag{5.51b}$$

$$\bar{\boldsymbol{\mu}}\left(\mathbb{X}_t\right) = \begin{bmatrix} 0 \\ \frac{1}{m+A_\infty}\sum_{m=1}^{M}\rho\left(\kappa_{1,m}^2 + \kappa_{0,m}\kappa_{2,m}\right)y_m \\ 0 \\ \vdots \\ 0 \end{bmatrix}. \tag{5.51c}$$

The drift array in (5.51a) is split into a linear component, $\hat{\boldsymbol{\mu}}$, which is matrix-multiplied by the state vector $\mathbb{X}_t$, and the nonlinear component, $\bar{\boldsymbol{\mu}}$. To reduce clutter, and in an attempt to highlight the structure of the system, we use the matrix $\overline{\boldsymbol{L}}$ for the κ-auxiliary-processes. The over-bar denotes the matrix minus the top entries contained in $\boldsymbol{\mu}_\zeta$. Lastly, the diffusion array is nonzero only for the seastate process

states,

$$\boldsymbol{\sigma} = \begin{bmatrix} 0 & \cdots & 0 & 0 & 0 & 0 \\ \vdots & \ddots & \vdots & \vdots & \vdots & \vdots \\ 0 & \cdots & \boldsymbol{\sigma}_{\zeta} & 0 & 0 & 0 \\ 0 & \cdots & \multicolumn{4}{c}{\multirow{3}{*}{$\overline{\boldsymbol{G}\,\boldsymbol{\rho}_{\zeta\kappa_q}}$}} \\ 0 & \cdots & & & & \\ 0 & \cdots & & & & \end{bmatrix} . \tag{5.52}$$

The nonzero structure of the diffusion array is intuitive, as the hydrodynamics and resulting vessel motions are deterministic, given the driving stochastic wave elevation process. Therefore, the stochastic evolution enters into the system only through the incident wave elevation. This is in part due to the properties associated with the selection of the Stratonovich stochastic integral.

Chapter 6

Numerical Approaches

We can take one of several approaches with the present seakeeping formulation to numerically compute the joint PDF of the seakeeping states. Two methods are outlined in this section: an SDE Monte-Carlo method, and the direct solution of the Fokker-Planck equation (2.17). While the Monte-Carlo method requires averaging statistics from a large ensemble of time-series simulations of the governing multidimensional SDE, (5.49), implementing it is straightforward. Alternatively, solving the FPE provides all the required information in one shot, at the cost of being significantly more computationally challenging, and as such, has the potential to be more time consuming in the nonlinear case. Furthermore, solving the FPE is considerably more complex in the non-stationary case.

6.1 SDE Monte-Carlo-Method

The Monte-Carlo approach with the SDE is conceptually identical to Monte-Carlo simulations deterministic systems, such as nonlinear panel methods, although the

novel formulation presented above offers significant advantages in the efficiency of computing response time-series. Recall the multidmensional system SDE in Stratonovich-array form (5.49),

$$d\mathbb{X}_t = \boldsymbol{\mu}\left(\mathbb{X}_t\right)\, dt + \boldsymbol{\sigma} \circ d\boldsymbol{W}_t \tag{6.1}$$

Calculating the joint-PDF of the states of $\mathbb{X}_t$ distills to calculating a histogram of the time-series simulations of $\mathbb{X}_t$, over an ensemble of simulations.

To simulate the ensemble of realizations of $\mathbb{X}_t$, a Stochastic-Stratonovich-Runge-Kutta-type scheme is employed as follows from Kloeden & Platten Section 12.3 equation (3.3) [24]. The discrete approximation $\bar{\boldsymbol{X}}_t$ for $\mathbb{X}_t$ is

$$\begin{aligned}\bar{\boldsymbol{X}}_{n+1} = \bar{\boldsymbol{X}}_n &+ \left[\alpha\boldsymbol{\mu}\left(\bar{\boldsymbol{X}}_{n+1}, t_{n+1}\right) + (1-\alpha)\,\boldsymbol{\mu}\left(\bar{\boldsymbol{X}}_n, t_n\right)\right] dt \\ &+ \frac{1}{2}\left[\boldsymbol{\sigma}\left(\boldsymbol{\Psi}_{\boldsymbol{n}}, t_n\right) + \boldsymbol{\sigma}\left(\bar{\boldsymbol{X}}_n, t_n\right)\right] \boldsymbol{dW}_n\end{aligned} \tag{6.2}$$

with the forward-Euler auxiliary component

$$\boldsymbol{\Psi}_n = \bar{\boldsymbol{X}}_n + \boldsymbol{\mu}\left(\bar{\boldsymbol{X}}_n, t_n\right)\, dt + \boldsymbol{\sigma}\left(\bar{\boldsymbol{X}}_n, t_n\right)\, \boldsymbol{dW}_n \tag{6.3}$$

where α is an "implicitness" parameter. This scheme has order 1 weak and strong convergence, the later of which we desire for convergence to physically-realistic results.

From Kloeden & Platten, the approximation $\bar{X}_t$ *converges in the weak sense* to $\mathbb{X}_t$ with order ε, if for any polynomial g, there exists a finite constant K and positive constant δ_0, such that

$$\left|E\left[g\left(X_T\right)\right] - E\left[g\left(\bar{X}_N\right)\right]\right| \leq K\delta^{\varepsilon}, \quad \delta \in (0, \delta_0) \tag{6.4}$$

for any temporal discretization with time step δ [24]. The weak convergence criterion is a statement on the approximation's convergence in distribution, whereby the discretize and exact SDE solution have the same probability distribution. But this convergence is limited for path-critical processes, such as in the seakeeping problem.

An approximation $\bar{X}_t$ *converges in the strong sense* with order ε, if there exists a finite constant K and positive constant δ_0, such that

$$E\left[|X_T - \bar{X}_N|\right] \leq K\delta^{\varepsilon}, \quad \delta \in (0, \delta_0) \tag{6.5}$$

When the SDE is deterministic, i.e. the diffusion $\sigma = 0$, the strong criterion reduces to the discrete-scheme convergence order criterion [24]. The strong convergence criterion is a statement that the time-path trajectories of the stochastic processes are sufficiently close to those of the exact SDE, and therefore the physical process (provided the SDE also converges sufficiently to the true deterministic physics). In the context of this problem, this condition ensures that the fairly abstract stochastic model does indeed generate realistic physical response trajectories. While we may be able to accept some degree of abstraction, ensuring strong convergence allows us to sanity-check simulations, not just in distribution, but by comparing the motion state trajectories against experimental or conventional numerical techniques.

A practical concern is how to generate the Wiener increment vector $\boldsymbol{dW}$. From the definition of a Wiener process (see Appendix A) [8],

1. $\mathbb{E}\left[\boldsymbol{dW}_t\right] = \mathbf{0}$

2. $\mathbb{E}\left[dW_{i,t}\, dW_{j,t}\right] = 0$

3. $\mathbb{E}\left[dW_{i,t} dW_{i,t}\right] = dt$

Therefore, $\boldsymbol{dW}_t = \mathcal{N}\left(0, \sqrt{dt}\right)$, or in MATLAB, $\sqrt{dt} * randn(N, N_t)$, where N_t is the number of time steps in the simulation.

If α is selected to be zero, the scheme is explicit, and looks like Forward-Euler,

$$\bar{\boldsymbol{X}}_{n+1} = \bar{\boldsymbol{X}}_n + \boldsymbol{\mu}\left(\bar{\boldsymbol{X}}_n, t_n\right) dt + \boldsymbol{\sigma} \boldsymbol{dW}_n \tag{6.6}$$

However, assuming the system is stiff, we take $\alpha = \frac{1}{2}$ results in a trapezoidal scheme,

$$\bar{\boldsymbol{X}}_{n+1} = \bar{\boldsymbol{X}}_n + \frac{1}{2}\left[\boldsymbol{\mu}\left(\bar{\boldsymbol{X}}_{n+1}, t_{n+1}\right) + \boldsymbol{\mu}\left(\bar{\boldsymbol{X}}_n, t_n\right)\right] dt + \boldsymbol{\sigma} \boldsymbol{dW}_n \tag{6.7}$$

Equation (6.7) results in a system of nonlinear equations at each time step for $\boldsymbol{X}_{n+1}$. We can easily solve this system by implementing a Newton-Raphson solver, using an initial guess $X_{t,0}$ provided by the explicit scheme (6.6). The objective function for the inner Newton loop is

$$\boldsymbol{F} = \bar{\boldsymbol{X}}_n - \bar{\boldsymbol{X}}_{n+1} + \frac{1}{2}\left[\boldsymbol{\mu}\left(\bar{\boldsymbol{X}}_{n+1}, t_{n+1}\right) + \boldsymbol{\mu}\left(\bar{\boldsymbol{X}}_n, t_n\right)\right] dt + \boldsymbol{\sigma} \boldsymbol{dW}_n = 0 \tag{6.8}$$

Note that in (6.8), the Wiener increment $\boldsymbol{dW}_n$ has a fixed and known value. Therefore, the corresponding update scheme is

$$\bar{\boldsymbol{X}}_{n+1}^{(j+1)} = \bar{\boldsymbol{X}}_{n+1}^{(j)} - \boldsymbol{J_F}^{-1}\left(\bar{\boldsymbol{X}}_{n+1}^{(j)}\right) \boldsymbol{F}\left(\bar{\boldsymbol{X}}_{n+1}^{(j)}\right) \tag{6.9}$$

where $\boldsymbol{J_F}$ is the Jacobian of the objective function (6.8). The update runs until a satisfactory convergence criterion is met. The imposed criterion is for the maximum error in any element of $\bar{\boldsymbol{X}}_{n+1}$ to be less than a specified tolerance. With this time-marching scheme, it is not hard to generate an ensemble of response path realizations, and to aggregate and compute their statistics, resulting in the desired PDF quantities for the seakeeping motion states.

To illustrate the time marching scheme, and also the stochastic seastate model, Figure 6-1 illustrates several methods of computing a wave elevation time series. We have selected a 2-term ESPRIT representation of the autocorrelation function with a peak frequency of $\omega_p = 0.5$ [rad/s] and a decay of $\lambda = 0.05$ [1/s], corresponding to a significant wave height of $H_S = 8.9$ [m]. The dashed-black curve uses the classical St Denis and Pierson seastate model, comprised of a superposition of 150 sinusoids with uniformly distributed random phases,

$$\zeta_{sD\&P}(t) = \sum_{n=1}^{150} \sqrt{2\Delta\omega S_\zeta(\omega_n)} \cos(\omega_n t + \varphi_n), \quad \varphi_n \in \mathrm{U}[0, 2\pi) \tag{6.10}$$

The dash-dot blue curve uses the Itô form of the seastate SDE, (5.5), using the Itô-analog of the explicit scheme (6.6), which is commonly known as the Euler-Maruyama scheme (i.e. stochastic extension of Forward-Euler). And the solid red line uses the Stratonovich seastate SDE (5.15) and the trapezoidal Runge-Kutta scheme (6.7). The two SDE schemes use the same Wiener increments at each time step, but from the figure, the important observation is that the generated wave elevation records look realistic, in addition to being probabilistically accurate. These simulations use a time step of $dt = 0.1$ [s]. We also draw attention to the "jaggedness" of the SDE records, which is an artifact of the driving unit white noise processes, which are continuous everywhere, but differentiable nowhere.

To illustrate the convergence of the simulation, we simulated an ensemble of 1000 realizations, each for a period of 600 seconds, and computed the averaged autocorrelation function for each method above, to compare to the input design spectrum, plotted in Figure 6-2). It is almost impossible to distinguish between the input (solid green), the St Denis and Pierson (dashed black) and the trapezoidal scheme (solid red). However, we can see as alluded to earlier, the error introduced

by using the Itô form of the SDE, and the fairly poor convergence of the Euler-Maruyama scheme for larger time steps.

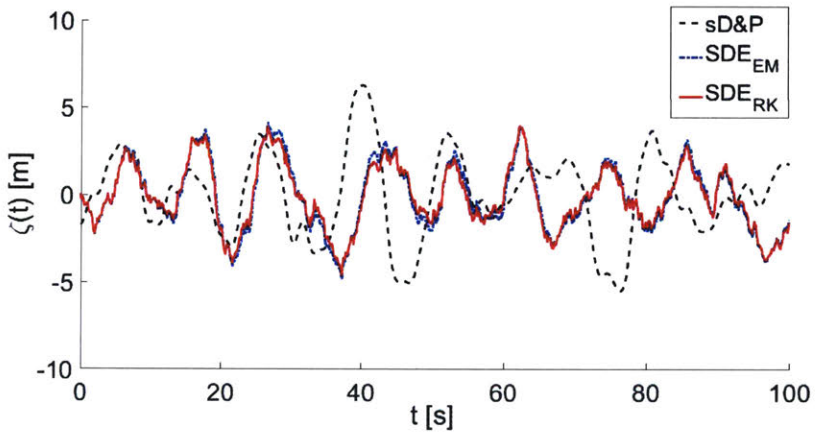

Figure 6-1: Simulated wave elevation records using St Denis and Pierson (dashed black), the Euler-Maruyama Itô scheme (dash-dot blue) and trapezoidal Runge-Kutta Stratonovich scheme (solid red) with a time step of $dt = 0.1$ [s]. All three yield realistic physical signals. Note the error between the Stratonovich trapezoidal scheme and the Itô Euler scheme.

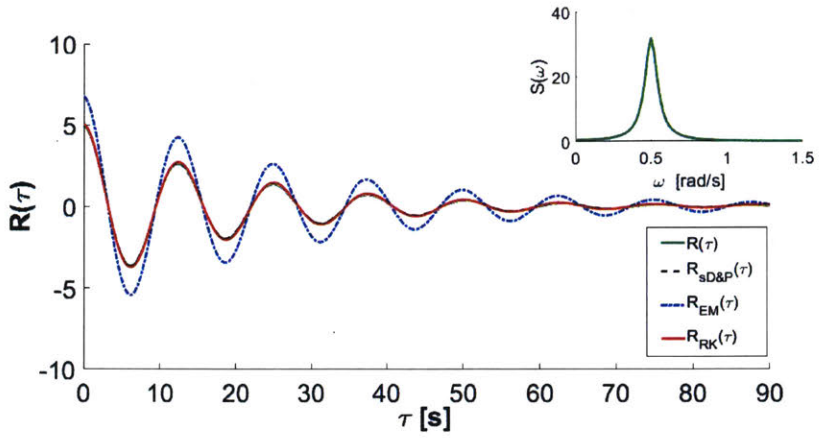

Figure 6-2: Averaged autocorrelation function over a 1000-realization ensemble using the St Denis and Pierson (dashed black), Euler-Maruyama Itô scheme (dash-dot blue) and trapezoidal Runge-Kutta Stratonovich scheme (solid red). Excellent graphical accuracy is seen between the design seastate (solid green) with the trapezoidal scheme SDE and St Denis and Pierson model. The Itô form does not converge well in this case for large time steps.

6.2 Numerical FPE Solution

Recalling that we wish to shortcut performing Monte-Carlo simulations of the responses, we will instead solve the corresponding FPE using a method proposed by Martens et. al. [25]. The procedure is reproduced here with the intent that it will be applied in future research phases.

Begin by assuming the stochastic system is stationary, $\frac{\partial p}{\partial t} = 0$. This method may be extended to non-stationary systems, but at the cost of considerably more complexity. However, we note that stationary solutions still provide significant insight on whether the vessel has lost stability, particularly with respect to a priori design criteria. If a stationary solution to the FPE does not exist for a vessel geometry and seastate, it may also indicate a loss of stability, although the nature and details of which would indeed require a proper transient solution.

Recalling the stationary Stratonovich FPE,

$$0 = -\sum_{i=1}^{N} \frac{\partial}{\partial x_i} \left[\mu_i \left(\boldsymbol{x}, t \right) p \left(\boldsymbol{x}, t \right) \right] + \frac{1}{2} \sum_{k=1}^{M} \sum_{i=1}^{N} \frac{\partial}{\partial x_i} \left\{ \sigma_{ik} \left(\boldsymbol{x}, t \right) \sum_{j=1}^{N} \frac{\partial}{\partial x_j} \left[\sigma_{jk} \left(\boldsymbol{x}, t \right) p \left(\boldsymbol{x}, t \right) \right] \right\} . \tag{6.11}$$

the proposed procedure is as follows [25]:

1. Find an appropriate approximate solution. This is chosen to be the linear system, and is used to generate Galerkin weighting functions.
2. Calculate an expansion basis of orthogonal generalized Hermite polynomials, with respect to the weighting functions determined in *Step 1.*
3. Calculate the residual to the FPE by introducing the expansion polynomials and weighting functions. The residual is a function only of the expansion polynomial outer-coefficients $C_{i_1 \ldots i_N}$. Solving for the coefficients in the context of a Galerkin-type procedure results in a homogenous linear system of equations for the coefficients. The coefficients are then inserted into the approximate solution, resulting in a Galerkin-approximation to the stationary joint PDF.

Beginning *Step 1* by assuming the system is linear, the output PDF is Gaussian. The differential equation for the covariance matrix $\mathbb{K}$ is again the Lyopunov-type equation,

$$\hat{\boldsymbol{\mu}} \mathbb{K} + \mathbb{K} \hat{\boldsymbol{\mu}}^T = -\boldsymbol{\sigma} \boldsymbol{\sigma}^T \tag{6.12}$$

This is similar to the calculation of the coupled wave substates we saw in Section 5.2.3. However, in this case, $\boldsymbol{\sigma}$ and $\hat{\boldsymbol{\mu}}$ are now known, and the covariance matrix $\mathbb{K}$ is the unknown term. Efficient solvers exist for (6.12), such as the MATLAB function *lyap*$(\cdot)$. The PDF of the linear solution follows,

$$\hat{p}\left(x_1, \ldots, x_N\right) = \frac{1}{(2\pi)^{N/2} \left|\mathbb{K}\right|^{1/2}} \exp\left[-\frac{1}{2}\boldsymbol{x}^T \mathbb{K}^{-1} \boldsymbol{x}\right] \tag{6.13}$$

The marginal probability densities are then used to generate decoupled Galerkin weighting functions $G^{(j)}\left(x_j\right)$ in the state-variables $\mathbb{X}$,

$$G^{(j)}\left(x_j\right) = \hat{p}_{x_j}\left(x_j\right) = \int_{-\infty}^{\infty} \cdots \int_{-\infty}^{\infty} \hat{p}\left(x_1, \ldots, x_N\right)\, dx_1 \cdots dx_{j-1}\, dx_{j+1} \cdots dx_N \tag{6.14}$$

Continuing to *Step 2*, the N weighting functions $G^{(j)}$ are used to generate a basis of polynomials of order k over $x_1, \ldots, x_N$

$$\mathbb{P}_k^{(j)}\left(x_j\right) = \sum_{i=0}^{k} a_{ki}^{(j)} x_j^i \tag{6.15}$$

where j varies from 1 to N, and k is an a priori specified order. The basis polynomial coefficients are given by applying the generalized Hermite orthogonality condition,

$$\int_{-\infty}^{\infty} \mathbb{P}_k^{(j)} \mathbb{P}_l^{(j)} G^{(j)}\left(x_j\right)\, dx_j = \begin{cases} c_k & k = l \\ 0 & k \neq l \end{cases} \tag{6.16}$$

where c_k is an arbitrary constant. The inner-coefficients $a_{ki}^{(j)}$ may be found by solving

the matrix equation

$$\begin{bmatrix} m_0^{(j)} & m_1^{(j)} & \dots & m_k^{(j)} \\ m_1^{(j)} & \ddots & & m_{k+1}^{(j)} \\ \vdots & & \ddots & \\ m_k^{(j)} & \dots & \dots & m_{2k}^{(j)} \end{bmatrix} \begin{bmatrix} a_{k0}^{(j)} \\ a_{k1}^{(j)} \\ \vdots \\ a_{kk}^{(j)} \end{bmatrix} = \begin{bmatrix} 0 \\ \vdots \\ 0 \\ \frac{c_k^{(j)}}{a_{kk}^{(j)}} \end{bmatrix} \tag{6.17}$$

using moments $m_\kappa^{(j)}$ with respect to the weighting function $G^{(j)}(x_j)$,

$$m_\kappa^{(j)} = \int_{-\infty}^{\infty} x_j^\kappa G^{(j)}(x_j)\, dx_j \tag{6.18}$$

Now knowing the orthogonal basis expansion inner-coefficients $a_{ki}^{(j)}$, an approximate PDF can be written in terms of the weighting functions and polynomial basis with outer-coefficients $C_{i_1 \dots i_N}$,

$$\tilde{p}(x_1, \dots, x_n) = \sum_{i_1=0}^{n_1} \cdots \sum_{i_N=0}^{n_N} C_{i_1 \dots i_N} \mathbb{P}_{i_1}^{(1)}(x_1) \cdots \mathbb{P}_{i_N}^{(N)} G^{(1)}(x_1) \cdots G^{(N)}(x_N) \tag{6.19}$$

The orders $n_1, \dots n_N$ determine the order of the approximate solution. These values may be less than or equal to the respective expansion order of the j-th polynomial basis, and are distinct to allow for lower expansion orders on weakly-nonlinear terms. All that remains is to determine the outer-coefficients $C_{i_1 \dots i_N}$.

Plugging in (6.19) into the FPE (2.17), and introducing the expansion polynomials for the state variables yields a residual in terms of the coefficients $C_{i_1 \dots i_N}$. This has been omitted until future work, as it is cumbersome but straightforward. The expression of this residual depends on the choice of the SDE model, number of

states, and expansion order. This residual will ultimately reduce, following somewhat involved standard algebraic manipulation, to a homogeneous system of linear equations, which is easily solved for $C_{i_1 \ldots i_N}$.

Finally, the coefficients $C_{i_1 \ldots i_N}$ are substituted back into (6.19), and the solution is complete. Inspecting the joint or marginal PDFs of the states yields the desired information to appropriately determine a Safe Operation Envelop for a defined seastate for a wide range of vessels. Thereby, the overall goal of the framework proposed herein is complete.

Chapter 7

Discussions & Future Work

7.1 Conclusion

We have presented a novel approach to the seakeeping problem, developed from the combination of Fluid Impulse Theory, ESPRIT-state-space formulation and applied stochastic analysis. The new theoretical framework casts the six-degree-of-freedom nonlinear seakeeping problem into a state-space form. This has permitted us to derive a multidimensional stochastic differential equation governing the system states driven by a vector of independent unit Wiener processes. From the SDE, we are able to derive the corresponding Fokker-Planck equation governing the joint probability density function of the states of the ship seakeeping problem. This model relies heavily on the attributes of Fluid Impulse Theory, along with standard panel methods, to compute the the hydrodynamic forces, illustrated for a rectangular barge in beam waves. Moreover the SDE representation of an ambient seastate governed by a known spectrum and probability density function has been illustrated.

A number of benefits are offered by the state-space representation of the nonlinear

seakeeping problem. It leads to an efficient a priori computation of wave memory effects in the form of a set of ESPRIT coefficients, which are time-invariant and generic with respect to the seastate for a specific vessel. Furthermore, it allows for the direct evaluation of the joint probability density function of the responses via the solution of the Fokker-Planck equation. By extending this model, additional nonlinear states may be added, representing effects such as viscous separated flow effects around bilge keels and the ship hull. It also permits the introduction of the standard machinery of optimal control theory that relies on the state-space representation of linear and nonlinear systems for the optimal steering of a vessel in a given seastate. The study of the attributes of the methodology we have introduced here will be the subject of future research.

7.2 Future Work

Studies moving forward aim to measure and validate the performance of this new methodology against experimental and deterministic computational methods for representative ship geometries in a range of seastates. A major question remaining surrounds the convergence and tradeoff in computational time between Monte-Carlo simulations of the nonlinear SDE and Galerkin-solutions of the large-dimension FPE. However, we expect that, as it stands, the model presented here has considerable computational and accuracy advantages in solving the nonlinear seakeeping problem, whether as an SDE or as a deterministic state-space system with an a priori wave elevation input.

Additionally, the illustrative formulations presented here have been expressed for two-dimensional roll motion. We aim to implement the complete coupled six-degree-of-freedom system, including large displacement motion, relaxing long wavelength

and small-steepness approximations, and studying admissibility of higher-order potentials. Additionally, more work is needed to understand the applicability of alternative definitions of stochastic integrals, and how their properties may increase or challenge the efficacy of this methodology.

Bibliography

[1] N. Umeda et. al. The specialist committee on stability in waves. Proceedings of the 25th ITTC, 2008.

[2] United Nations Conference on Trade and Development. Review of Maritime Transport 2017. United Nations Publication, 2017.

[3] M. K. Ochi. Ocean Waves: The Stochastic Approach. Cambridge Ocean Technology Series. Cambridge University Press, 1998.

[4] P. D. Sclavounos. 2.24: Ocean Wave Interaction with Ships and Offshore Energy Platforms Lecture Notes. MIT CopyTech, 2017.

[5] V. Belenky, K. Weems, and W.-M. Lin. Split-time method for estimation of probability of capsizing caused by pure loss of stability. Ocean Engineering, 122:333 – 343, 2016.

[6] V. Campbell, V. Belenky, and V. Pipiras. Application of the envelope peaks over threshold (epot) method for probabilistic assessment of dynamic stability. Ocean Engineering, 120:298 – 304, 2016.

[7] P. D. Sclavounos. Nonlinear impulse of ocean waves on floating bodies. Journal of Fluid Mechanics, 697:316–335, April 2012.

[8] B. Øksendal. Stochastic Differential Equations: An Introduction with Applications. Universitext. Springer-Verlag, Berlin Heidelberg, 6 edition, 2003.

[9] R. Stratonovich. A New Representation for Stochastic Integrals and Equations. SIAM Journal on Control, 4(2):362–371, May 1966.

[10] E. Wong and M. Zakai. Riemann-Stieltjes approximations of stochastic integrals. Zeitschrift fr Wahrscheinlichkeitstheorie und Verwandte Gebiete, 12(2):87–97, June 1969.

[11] A. D. Fokker. Die mittlere Energie rotierender elektrischer Dipole im Strahlungsfeld. Annalen der Physik, 348(5):810–820, 1914.

[12] A. Kolmogoroff. ber die analytischen Methoden in der Wahrscheinlichkeitsrechnung. Mathematische Annalen, 104(1):415–458, December 1931.

[13] H. C. Öttinger. Stochastic Calculus. In Stochastic Processes in Polymeric Fluids, pages 81–148. Springer, Berlin, Heidelberg, 1996.

[14] Z. Yu and J. Falnes. State-space modelling of a vertical cylinder in heave. Applied Ocean Research, 17(5):265 - 275, 1995.

[15] T. Perez and T. I. Fossen. Practical aspects of frequency-domain identification of dynamic models of marine structures from hydrodynamic data. Ocean Engineering, 38(2):426 - 435, 2011.

[16] H. B. Bingham. Simulating ship motions in the time domain. Thesis, Massachusetts Institute of Technology, 1994.

[17] D. Potts and M. Tasche. Parameter estimation for nonincreasing exponential sums by Prony-like methods. Linear Algebra and its Applications, 439(4):1024 - 1039, 2013.

[18] C. Casanovas. Advanced controls for floating wind turbines. Thesis, Massachusetts Institute of Technology, 2014.

[19] S. L. Primak and V. Z. Lyandres. On the generation of the baseband and narrowband non-Gaussian processes. IEEE Transactions on Signal Processing, 46(5):1229–1237, May 1998.

[20] S. Primak, V. Kontorovich, and V. Lyandres. Synthesis of Stochastic Differential Equations. In Stochastic Methods and Their Applications to Communications, pages 321–375. John Wiley & Sons, Ltd, 2004.

[21] S. M. Rytov, Y. A. Kravtsov, and V. I. Tatarskii. Principles of Statistical Radiophysics 2: Correlation Theory of Random Processes. Springer-Verlag, Berlin Heidelberg, 1988.

[22] N. Wiener. The Linear Predictor for a Single Time Series. In Extrapolation, Interpolation, and Smoothing of Stationary Time Series: With Engineering Applications, pages 176–. MIT Press, 1949.

[23] J. C. Jimenez. Simplified formulas for the mean and variance of linear stochastic differential equations. arXiv:1207.5067 [math], July 2012. arXiv: 1207.5067.

[24] P. E. Kloeden and E. Platen. Numerical Solution of Stochastic Differential Equations. Stochastic Modelling and Applied Probability. Springer-Verlag, Berlin Heidelberg, 1992.

[25] W. Martens, U. von Wagner, and V. Mehrmann. Calculation of high-dimensional probability density functions of stochastically excited nonlinear mechanical systems. Nonlinear Dynamics, 67(3):2089–2099, February 2012.

Appendices

Appendix A

Stochastic Integration & Differential Equations

The concept of the stochastic integral and stochastic differential equation is briefly introduced. The basic mathematical background and preliminaries are assumed known. For more detail, the reader is referred to Øksendal (2010) [8].

Consider a set Ω, and a σ-algebra $\mathcal{A}$ on Ω, the resulting pair $(\Omega, \mathcal{A})$ is a *measurable space*. A probability measure P is defined on the measurable space $(\Omega, \mathcal{A})$, $P : \mathcal{A} \rightarrow [0, 1]$. The triple $(\Omega, \mathcal{A}, P)$ is therefore called a *probability space*.

A *random variable* is a measurable function $Y :\rightarrow \mathbb{R}^n$ over the probability space $(\Omega, \mathcal{A}, P)$. And a *stochastic process* is a parameterized collection of random variables, $\{X_t\}_{t \in T}$ defined on $(\Omega, \mathcal{A}, P)$. In the context of this work, the parameter t may be thought of as "time," and each ω is a realization or single "experiment" of the process $X_t(\omega)$.

An important fundamental process to define is the Brownian motion process, otherwise known as the unit Wiener process, $W_t(\omega)$. The construction is omitted

here, but key properties are:

1. $W_{t=0} = 0$ almost surely.

2. W_t is a *Gaussian* process. For all $0 \leq t_1 \leq \ldots \leq t_s$, the random variable $Z = (W_{t_1}, \ldots, W_{t_s}) \in R^{ns}$ has a normal distribution.

3. W_t has *independent increments*: $W_{t_1}, W_{t_2} - W_{t_1}, \ldots$ are independent $\forall 0 \leq t_1 < \cdots < t_s$.

4. $W_t(\omega)$ is almost surely *continuous* for almost all ω, by Kolmogorov's continuity theorem.

5. The quadratic variation of W_t is $[dW_t dW_t] = dt$.

A.1 The Stochastic Integral

The Itô stochastic integral defining a stochastic process X_t, may be constructed by considering the discrete sum

$$X_{s+1} - X_s = \mu(t_s, X_s)\Delta t_s + \sigma(t_s, X_s) B_s \Delta t_s \tag{A.1}$$

$$\Delta t_s = t_{s+1} - t_s \; ; \quad B_s = B_{t_s} \; .$$

where B_s is a fundamental "noisy" stochastic process that drives the process X_t. $B_s \Delta t_s$ can be replaced with $\Delta U_s = U_{s+1} - U_s$, which is the increment of some arbitrary stochastic process U_t satisfying the requirement that it have *stationary independent increments, each with mean zero.* The only such process satisfying these

requirements in the increment is the Wiener process, $U_s = W_s$, and therefore, (A.1) is re-written as

$$X_{s+1} = X_0 + \sum_{j=0}^{s} \mu\left(t_j, X_j\right) \Delta t_j + \sum_{j=0}^{s} \sigma\left(t_j, X_j\right) \Delta W_j \; . \tag{A.2}$$

Taking the limit as $\Delta t \to 0$ permits the use of the familiar integral notation,

$$X_t = X_0 + \int_0^t \mu\left(s, X_s\right) ds + \int_0^t \sigma\left(s, X_s\right) dW_s \tag{A.3}$$

The first term on the right-hand side of (A.3) is a standard Riemann integral with respect to the dummy time variable ds. The second term is the Itô stochastic integral, integrated against the stochastic process dW, the "white noise process," satisfying the properties above. The detailed properties of this integral are left to other resources, however, it is important to note in the context of applications to the physics presented above, that the process X_t is an adapted process, i.e. it only has knowledge of present and past values, and may not anticipate anything in the future.

The process generated by (A.3) satisfies the differential equation

$$dX_t = \mu\left(t, X_t\right) dt + \sigma\left(t, X_t\right) dW_t \; . \tag{A.4}$$

Equation (A.4) is thus called an "Itô stochastic differential equation." Imagine there is a scalar function of the process $f : X_t \to Y_t$. If one to write down the differential equation of the process Y_t, caution must be exercised, as the ordinary calculus chain rule does not apply. Instead, one must apply Itô's Lemma for a scalar process [8],

$$df = \left(\frac{\partial f}{\partial t} + \mu_t \frac{\partial f}{\partial x} + \frac{\sigma_t^2}{2} \frac{\partial^2 f}{\partial x^2}\right) dt + \sigma_t \frac{\partial f}{\partial x} dW_t \tag{A.5}$$

The multi-dimensional form of (A.5) is considerably more complex,

$$df\left(t, \boldsymbol{X}_t\right) = \left\{ \frac{\partial f}{\partial t} + \left(\nabla_{\boldsymbol{X}} f\right)^T \boldsymbol{\mu}_t + \frac{1}{2}\mathrm{Tr}\left[\boldsymbol{\sigma}_t^T \left(\mathbb{H}_{\boldsymbol{X}} f\right) \boldsymbol{\sigma}_t\right] \right\} dt + \left(\nabla_{\boldsymbol{X}} f\right)^T \boldsymbol{\sigma}\, \boldsymbol{dW}_t \quad \text{(A.6)}$$

where $\mathrm{Tr}(\cdot)$ is the trace operator and $\mathbb{H}_{\boldsymbol{X}}$ denotes the Hessian of f. We see that functions of stochastic diffusions may be become cumbersome to unwieldy when taking derivatives, and furthermore is rather unintuitive.

However, there are several alternative definitions of stochastic integrals to (A.3). One in particular, the Stratonovich stochastic integral, is important to the present work. Note the discrete Itô sum in (A.2) is a left-endpoint approximation to X_t. The Stratonovich form is defined in an analogous way, using a midpoint approximation to X_t [9],

$$X_{s+1} = X_0 + \sum_{j=0}^{s} \mu\left(t_j, X_j\right) \Delta t_j + \sum_{j=0}^{s} \sigma\left(\left(\frac{X_{j+1} + X_j}{2}\right), t_j\right) \Delta W_j \,. \quad \text{(A.7)}$$

Equation (A.7) is represented in integral notation by

$$X_t = X_0 + \int_0^t \mu\left(s, X_s\right) ds + \int_0^t \sigma\left(s, X_s\right) \circ dW_s \,, \quad \text{(A.8)}$$

where $\circ$ denotes a Stratonovich integral. The corresponding differential equation is

$$dX_t = \mu\left(t, X_t\right) dt + \sigma\left(t, X_t\right) \circ dW_t \,. \quad \text{(A.9)}$$

A key useful property of the Stratonovich form is that the higher-order terms in Itô's Lemma cancel, leading to the conclusion that the Stratonovich integral obeys the ordinary calculus chain rule.